
Characterization and Design of a Readout Circuit for a Piezoelectric-based Acoustic Disdrometer



Submitted to the Office of Graduate Studies of the Delft University of Technology
In partial fulfillment of the requirements for the degree of
MASTER OF SCIENCE

In

Faculty of Electrical Engineering, Mathematics and Computer Science
(Department of Microelectronics)

by

Ravi Bagree
born in Bikaner, India

Supervisor: Prof. K. A. A. Makinwa



Electronic
Instrumentation
Laboratory



Ravi Bagree
Electronic Instrumentation Group,
Faculty of EEMCS,
Mekelweg 4,
Delft 2628 CD
The Netherlands



Copyright © 2012 by Ravi Bagree

All rights reserved.

No part of the material protected by this copyright notice may be reproduced or utilized in any form or by any means, electronic or mechanical, including photocopying or by any information storage and retrieval system, without permission from this publisher.

Printed in The Netherlands

*To my brother, Aashish
And my family, for their love*

Characterization and Design of a Readout Circuit for a Piezoelectric-based Acoustic Disdrometer

Author: Ravi Bagree
Student Id: 4046943
Email: r.bagree@student.tudelft.nl

Abstract

In 2009, Department of Water Management (DWM) at TU Delft conceptualized the design of a low-cost disdrometer suitable for large scale, remote deployment. But, being a novel idea, its electrical characteristics were not well researched. Also, the system was not sensitive enough to measure the raindrops of diameter less than 0.9mm. Furthermore, it was found that the proposed disdrometer suffers from the edge effect i.e. when a raindrop hits on the edge of the disdrometer; the size of the raindrop is underestimated. All the aforementioned issues have been addressed in this research.

The presented work discusses the electrical characteristics of the disdrometer. A readout circuit has been designed to improve the performance of the disdrometer and an innovative technique has been developed to solve the problem of edge effect.

The impedance response of the disdrometer has been analyzed and an equivalent electrical model of the proposed disdrometer has been developed and characterized. Furthermore, an elaborative analysis of the edge effect has been presented. Based on this analysis, an innovative technique has been proposed for reducing the edge-effect. This technique uses the envelope of the transducer's output to determine if the drop hit on edge. Also, a low-power (17.8mA@5V), low-noise ($7.8\mu\text{V}_{\text{rms}}$) readout circuit has been designed. This readout circuit is able to measure the drops of size as low as 0.4mm.

Because of the achieved results, this disdrometer is attracting a lot of attention of various groups from industry as well as from academia. A group of researchers from the DWM, TU Delft is looking forward to turn it in to a commercial product.

Thesis Committee

Chair and Supervisor: Prof. Dr. K. A. A. Makinwa, EEMCS, TU Delft
Committee Member: Prof. Dr. P. J. French, EEMCS, TU Delft
Committee Member: Dr. R. B. Staszewski, EEMCS, TU Delft

Acknowledgment

Although I have spent numerous hours to complete this thesis yet it would not have been possible without the support and guidance of various people. I take this opportunity to express my gratitude towards all such wonderful people.

First of all, I would like to acknowledge my supervisor Prof Kofi Makinwa for giving me this wonderful opportunity to work on such an interesting project. I always wanted to work on a project of social importance and his project has provided me exactly what I was looking for.

I would also like to thank my daily supervisor Dr. Youngcheol Chae for his immense support and for always being available. Even at times, when I slacked in my work, he was there to push me and inspire me to give my best.

I am also very thankful to Dr. Anton Bakker for reviewing my thesis and giving so many valuable comments. Without his support it would have been very difficult to complete this report.

I also take this platform to thank Rolf Hut and Stijn de Jong for their enormous support throughout the thesis. The disdrometer used in this thesis has been designed by Stijn. The application of this sensor is in the area of hydrology and water management which was unknown to me before this project. Through various technical and non-technical discussions they helped me in understanding the disdrometer and its target applications. Also, I used the measurement setup developed by Stijn. I would like to thank him for all the support he gave during the measurements.

It was my good fortune to have had a great set of students whom I shared the students' lab with. I would like to thank Gaurav, Shishir, Bharani, Ali, Junfeng, Zeng and Nandish for providing a congenial environment for me to work at. It was great to have them in the same room as much for the technical discussions as for the fun.

I would also like thank Maruti, Vishwas and Venkat for reviewing my thesis. I am overwhelmed with the kind of support they gave me in reviewing my thesis, especially Maruti. Without their help it would have been impossible to write this dissertation.

I would also like to thank Dhariyash, Shekhar, Vishwas and Abhijit for their care and support at home. Especially, I appreciate their patience to put up with my laziness. I also thank Ankit and Meghal for all the fun I had playing "*Ludo*" and "*Twenty-nine*".

But, most importantly I am very grateful to my family, especially my brother. Whatever I have achieved in my life, I owe it to them. They never let me see through the numerous sacrifices they made and hardships they went through for me. Staying away from your family is never an easy task. But a gang of as wonderful friends as Abhijit, Abhishek, Ali, Ankit, Apurva Bharani, Dhariyash, Gaurav, Maruti, Meghal, Priyanka, Rachit, Rahul, Shagun Shekhar, Shishir, Shreyash, Venkat, Vishwas..., always make you say "*Aaall izzzzz well*".

Table of Contents

Abstract.....	iii
Acknowledgment.....	v
Table of Contents.....	vii
List of Figures.....	ix
List of Tables.....	xi
Chapter 1 Introduction.....	1
1.1 Motivation.....	1
1.2 Disdrometer and Applications.....	1
1.2.1 Applications.....	1
1.3 Traditional Methods of Drop Size Measurement.....	3
1.4 Disdrometer Principle and State-of-Art.....	3
1.4.1 Displacement Disdrometer.....	4
1.4.2 Optical Disdrometer.....	5
1.4.3 Acoustic Disdrometer.....	7
1.4.4 Summary.....	9
1.5 Low-Cost Disdrometer by DWM.....	10
1.6 Thesis Organization.....	12
Chapter 2 Measurand and Transducers.....	13
2.1 Raindrop Characteristic.....	13
2.1.1 Formation of Raindrops.....	13
2.1.2 Shape and Size of Raindrop.....	13
2.1.3 Terminal velocity.....	14
2.1.4 Momentum of a raindrop.....	15
2.1.5 Drop Size Distribution (DSD).....	15
2.2 Transduction Principle.....	16
2.2.1 The Piezoelectric Effect.....	17
2.2.2 Piezoelectric Ceramics.....	17
2.3 Conclusion.....	21
Chapter 3 Sensor Modeling and Characterization.....	23
3.1 Proposed Sensor System.....	23
3.1.1 Hat of the sensor.....	24
3.1.2 Piezoelectric Diaphragm.....	25
3.2 Transducer Modeling.....	28
3.2.1 Impedance Characteristics of PED.....	28
3.2.2 Impedance characteristic of packaged PED.....	29
3.2.3 Equivalent Electric circuit Model.....	30

3.3 Signal Generation.....	33
3.3.1 Drop ball Setup	35
3.4 Transfer function for the disdrometer	36
3.4.1 Coherent results	37
3.4.2 Drop Tower Setup.....	37
3.5 Edge Effect.....	39
3.5.1 Solution to edge effect	40
3.5.2 Depth of the Edge Effect.....	41
3.6 Summary	42
Chapter 4 Circuit Design and Measurements	43
4.1 Specifications	43
4.1.1 Dynamic Range.....	43
4.1.2 Bandwidth	44
4.1.3 Noise	44
4.1.4 Power	44
4.1.5 Specifications Summary	45
4.2 Measurement Setup.....	45
4.3 System Architecture.....	47
4.3.1 Amplifier.....	47
4.3.2 Analog-to-Digital Converter (ADC).....	50
4.3.3 Proposed Circuit Design	50
4.4 Component Selection	51
4.4.1 Amplifier – LMV851 [42]	51
4.4.2 Analog-to-Digital Converter (ADC) – AD7767-2 [43].....	51
4.4.3 Voltage Reference (V_{ref})-MAX6126 [44].....	52
4.4.4 Passive components	52
4.5 PCB Design.....	52
4.6 Measurements Results	55
4.6.1 Power Consumption.....	55
4.6.2 Noise Measurements of readout circuit	55
4.6.3 System Noise Performance	55
4.6.4 Reproducibility of a fixed impact point.....	56
4.6.5 Transfer Function.....	57
4.6.6 Small drop output signal	58
Chapter 5 Contributions and Recommendations	61
5.1 Original Contributions	61
5.2 Future Recommendations	62
Appendix A: Edge Detection Algorithm	63
Appendix B: Dynamic Range of the System	67
Appendix C: Analysis of Available Power Budget	69
Appendix D: Noise Analysis of the System	71
Bibliography	75

List of Figures

Figure 1.1 Distribution of raindrops for a rain intensity of 10 mm h^{-1}	2
Figure 1.2 Types of disdrometers	3
Figure 1.3 Schematic of displacement disdrometers	4
Figure 1.4 Joss-Waldvogel disdrometer based on impact disdrometer principle [5]	4
Figure 1.5 Schematic of optical disdrometer [8]	6
Figure 1.6 Thies Clima laser precipitation monitor based on optical disdrometer principle [9]	6
Figure 1.7 Schematic of acoustic disdrometer	7
Figure 1.8 Vaisala RainCap disdrometer based on acoustic disdrometer principle [11]	8
Figure 1.9 DWM disdrometer [2]	10
Figure 1.10 Comparing the calculated rainfall rate given by disdrometer with standard tipping bucket for heavy rainfall [13]	10
Figure 1.11 Comparing the calculated rainfall rate given by disdrometer with standard tipping bucket for light rainfall ($< 5 \text{ mm/hr}$) [13]	11
Figure 2.1 (a) Shapes of raindrops [16], (b) equivolume diameter of raindrops [15]	14
Figure 2.2 Drop Size Distribution for raindrops during rainfall [21]	16
Figure 2.3 Example of piezoelectric effect [23]	17
Figure 2.4 Polarization of ceramic material [23]	18
Figure 2.5 Tensor notations for piezoceramic material [2]	18
Figure 3.1 Schematic of prototypes: (a) designed by Degen, (b) designed by Stijn [2]	23
Figure 3.2 Hat of the disdrometer: (a) side view, (b) bottom view, (c) with PED	24
Figure 3.3 Puddle effect: accumulation of water on the hat of the disdrometer	25
Figure 3.4 Puddle effect on new hat (a) new hat with soft edge, (b) puddle effect on new hat	25
Figure 3.5 Piezoelectric diaphragm (a) PED used by Stijn [2] (b) construction of a PED [48]	26
Figure 3.6 Impedance response of the given PED over a frequency range of $100 \text{ Hz} - 10 \text{ KHz}$	28
Figure 3.7 Impedance response of the given disdrometer over a frequency range of $100 \text{ Hz} - 10 \text{ kHz}$	29
Figure 3.8 Partition of phase response of the given disdrometer into low frequency non-resonant part and high frequency resonant part over a frequency range of $100 \text{ Hz} - 10 \text{ KHz}$	30
Figure 3.9 Van Dyke's model for a piezoelectric element at resonance [28]	30
Figure 3.10 Model proposed by Guan for the non-resonant part of the frequency [33]	31
Figure 3.11 Equivalent model of the disdrometer [33]	31
Figure 3.12 Equivalent model of disdrometer with components values	32
Figure 3.13 Simulated result of the equivalent model of disdrometer	32
Figure 3.14 Transfer of momentum: (a) raindrop starts falling at $t < 0$, (b) raindrop touches the sensor's surface at $t_s \geq 0$, (c) raindrop get spread in time $t_e > 0$, (d) surface starts oscillating [36]	33
Figure 3.15 Output signal of PED for a raindrop	34
Figure 3.16 Drop ball setup (a) first design (b) second design	35
Figure 3.17 Steel ball's momentum vs peak output voltage	36

Figure 3.18 Coherence between the output of steel ball impact and raindrop impact (a) disdrometer's output for steel ball impact (b) disdrometer's output spectrum for steel ball impact (c) disdrometer's output for raindrop impact (d) disdrometer's output spectrum for raindrop impact	37
Figure 3.19 Schematic of the drop tower setup in CiTG, TU Delft.....	38
Figure 3.20 Output result of the drop tower experiment	38
Figure 3.21 Schematic representation of edge effect.....	39
Figure 3.22 Disdrometer output signal of drop impact (a) away from the edge, (b) on the edge...	40
Figure 3.23 Transfer of momentum between a raindrop and DWM Disdrometer (a) drop impinges at the center, (b) drop impinges on the edge.....	41
Figure 3.24 DWM disdrometer to test the depth of edge effect	41
Figure 3.25 Schematic representation of the extent edge effect on PED.....	42
Figure 4.1 Measurement setup.....	45
Figure 4.2 The remote part of the measurement setup.....	46
Figure 4.3 Measurement setup.....	46
Figure 4.4 Typical sensor readout system.....	47
Figure 4.5 Charge mode amplifier circuit.....	47
Figure 4.6 Frequency response of charge mode amplifier.....	48
Figure 4.7 Voltage mode amplifier circuit.....	49
Figure 4.8 Frequency response of the voltage mode amplifier.....	49
Figure 4.9 A simplified schematic of the proposed circuit.....	50
Figure 4.10 Frequency response of the proposed circuit at amplifier output	51
Figure 4.11 Schematic of the readout circuit	53
Figure 4.12 Layout of PCB	54
Figure 4.13 Designed PCB for the DWM disdrometer.....	54
Figure 4.14 Readout circuit noise at ADC's output	55
Figure 4.15 Noise performance of the disdrometer	56
Figure 4.16 Reproducibility of disdrometer's output	57
Figure 4.17 Result of drop tower measurements with new setup.....	58
Figure 4.18 Disdrometer output for drops of size 0.3mm - 0.5mm along diameter	58
Figure A.1 Output of the DWM disdrometer for a drop hitting near the center of the sensor.....	63
Figure A.2 Output of the DWM disdrometer for a drop hitting at the edges of the sensor.....	64
Figure A.3 Output of the DWM disdrometer for a good drop demonstrating the sharp hike in the function $f(x)$	65
Figure D.1 Noise equivalent circuit of the proposed design.....	71

List of Tables

Table 1-1 Specifications for JWD [6]..... 5
Table 1-2 Specifications for LPM disdrometer [9]..... 7
Table 1-3 Specifications of Vaisala RainCap [12] 8
Table 1-4 Comparison of the presented disdrometers 9
Table 1-5 Target specifications for a new disdrometer 9
Table 4-1 System Specification 45
Table 4-2 Drop peak voltage for reproducibility test..... 57
Table 5-1 Comparison with the commercially available disdrometer 62

Chapter 1 Introduction

1.1 Motivation

In 2008, Delft University of Technology (TUD) and Oregon State University started the project “Trans-African Hydro-Meteorological Observatory” (TAHMO) [1]. It aims to foster better understanding of the African environment, through participatory sensing, modeling and education. One of the objectives of this project is to create a network of 20,000 hydro-meteorological stations in Africa by 2015. The data obtained by this network will be combined with models and satellite observations in order to get an insight into the distribution of water and energy stocks within Africa.

A hydro-meteorological station measures climate parameters such as temperature, humidity, wind speed/direction, rain rate and precipitation. Many instruments are commercially available for measuring these parameters, but they are cost prohibitive. To make the TAHMO project feasible, the cost of each station should be less than US \$200. Also, the station’s power consumption needs to be low enough to be powered by solar panel. It requires novel measures to make such an ambitious project possible. As a first step, it was decided to develop a low-cost and low-power rain gauge.

Various rain gauges like tipping bucket, weighing rain gauge and optical rain gauge are commercially available in the market. But they are either power hungry or require frequent maintenance, which makes them unsuitable for use in TAHMO. In [2], an innovative rain gauge was proposed by the Department of Water Management (DWM) at TUD. It is based on a simple piezoelectric transducer. Being a newly invented instrument, the electrical characteristics of the proposed rain gauge needed further investigation. The aim of this project is to do this and also to design a low power readout circuit for it.

1.2 Disdrometer and Applications

The proposed rain gauge is actually a disdrometer. This is an instrument that measures the size of a rain drop and records it for future analysis. In other words, it is a special kind of rain gauge, which collects information about each raindrop.

1.2.1 Applications

A disdrometer can be used for various purposes, e.g. meteorological measurements, prediction of soil erosion and radar technology. The output of a disdrometer is used to study the distribution of the size of raindrops during a rain event. Parameters such as rainfall intensity, kinetic energy of rainfall can be conveniently computed, based on this distribution. Figure 1.1 shows an example of such a distribution.

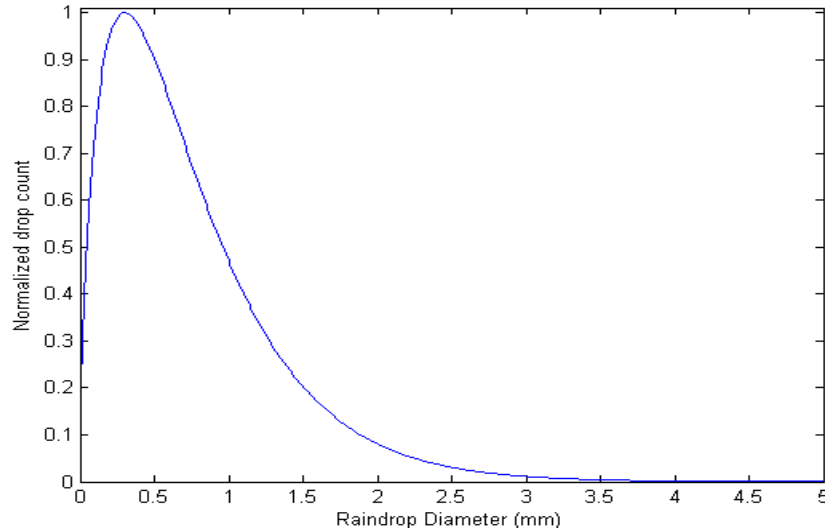


Figure 1.1 Distribution of raindrops for a rain intensity of 10 mm h^{-1}

Some of the popular applications of a disdrometer are as follows:

Meteorology

A disdrometer can be used as a rain gauge. Parameters such as rain intensity and rain depth can be computed at any time instant by integrating the volume of raindrops over a period of time.

Prediction of Soil Erosion

Information about the size of a raindrop is of crucial importance for research on soil erosion caused by rainfall. The impact of a raindrop has an important effect on soil erosion, aggregate soil breakdown and infiltration. It has been observed that large raindrops induce more erosion than smaller drops [3]. Therefore, information about the distribution of raindrop size is required to study and predict the soil erosion.

Microwave Communication

Radio communication is another application where the effect (attenuation of microwave signal) of rain is important. The effect of rain on microwave propagation is highly non-linear with respect to raindrop size and rainfall intensity. Telecommunication companies spend millions of dollars to maintain stable and efficient radio links. The increasing application of wireless technology makes it important to accurately consider the accurate impact of rain on such communication links.

Radar Technology

The distribution of raindrop size is of great interest for radar technology. The size of raindrops and their concentration information can be used to determine the reflectivity of a cloud. Various characteristics of precipitating clouds, such as microwave irradiance, cloud-top infrared irradiance and radar reflectivity can be remotely measured with the help of this information.

1.3 Traditional Methods of Drop Size Measurement

In the last century, much work has been devoted to the design and development of instrument to measure the size of raindrops. More than a century old reports can be found on this subject. Several unconventional methods like dye stains, flour pellets, oil immersion, aluminum foil [4] have been used to measure the size of a raindrop. But these methods had the intrinsic disadvantage of being labor intensive and only worked properly for sparse raindrops. Since rain intensity is not constant during a rain event and varies with time, these methods lead to erroneous conclusions/measurements. These limitations have motivated the need for better measurement methods which are continuous in nature.

1.4 Disdrometer Principle and State-of-Art

With the recent advancements in technology, several novel disdrometers have been proposed and are commercially available. Depending on the principle of operation, disdrometers fall into two major categories:

1. Impact Disdrometers
2. Optical Disdrometers

Impact disdrometers are based on the mechanical interaction between the transducer and a raindrop. Based on the transduction phenomenon used, impact disdrometer can further be categorized into:

1. Displacement Disdrometers
2. Acoustic Disdrometers

This section describes the working principle of displacement, acoustic and optical disdrometers. For each category, an example of a commercially available product is also given.

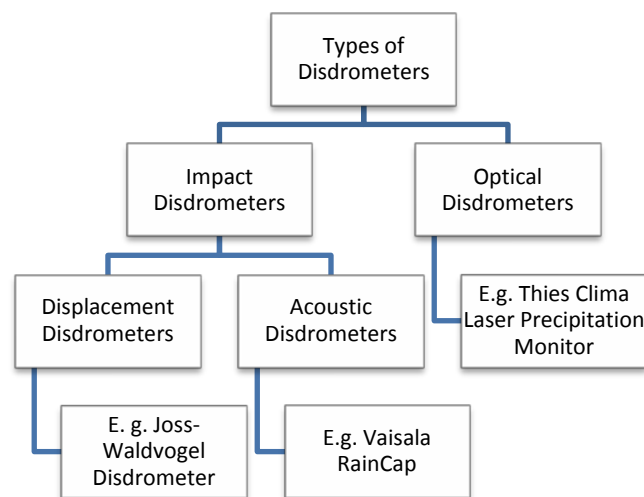


Figure 1.2 Types of disdrometers

1.4.1 Displacement Disdrometer

Figure 1.3(a) shows a schematic of a displacement disdrometer. It is an electromechanical unit with a vertical moving top surface. As shown in Figure 1.3(b), a raindrop impinging on the top surface transfers its mechanical energy to the disdrometer. As a result, the top surface is displaced and gains vertical momentum. Via magnetic induction, the vertical motion of the disdrometer surface can be used to extract information about the size of a raindrop.

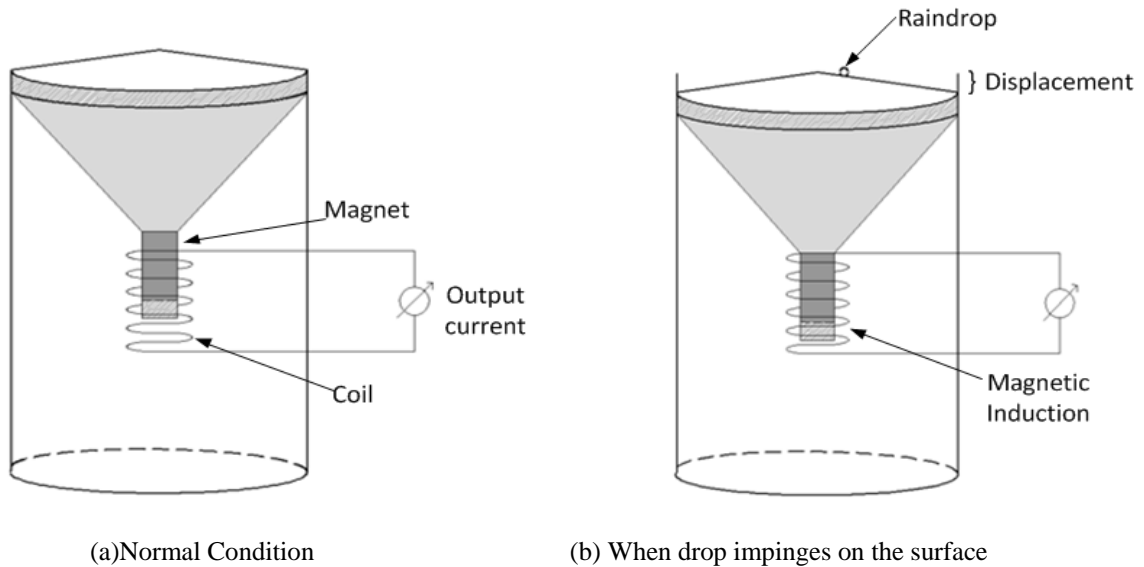


Figure 1.3 Schematic of displacement disdrometers

Joss-Waldvogel Disdrometer [5]

Figure 1.4 shows an example of a widely-used displacement disdrometer: the Joss-Waldvogel Disdrometer (JWD). By using a magnetic induction and compensation principle, it converts the displacement produced by an individual drop into raindrop size.



Figure 1.4 Joss-Waldvogel disdrometer based on impact disdrometer principle [5]

The JWD consists of three parts: a Styrofoam membrane, an outer cylinder with two coils at the bottom and an inner central column with a magnet on the base. The two coils are located around the lower part of the outer cylindrical column. A magnet, which is attached to the central column, is allowed to move freely in the vertical axis. When a raindrop impinges on the membrane, the central column, and hence the magnet, move through the coils. Movement of the magnet induces a current into the coil. Now, the size of the raindrop can be extracted by applying signal conditioning to the induced current.

The JWD consists of two separate units: a Sensor and a Processor. The specifications for these two units are given in Table 1-1.

Table 1-1 Specifications for JWD [6]

Parameters	Sensor Unit	Processor Unit	Total
Range (along diameter)	0.3 mm to 5 mm	-	-
Resolution	127 classes		
Sampling Area	50 cm ²	-	-
Approximate Cost (USD)	\$ 5,000	\$ 7,000	\$ 12,000[7]
Weight	2.9 Kg	2.2 Kg	5.1Kg
Dimensions	10 x 10 x 17 cm ³	12 x 26 x 27 cm ³	-
Power	-	-	115/230 Volts AC, 5.5 VA, (9 to 18 Volts DC; 3.3 Watts, also possible)

Here, the resolution is defined as the number of classes into which the drops can be classified.

From Table 1-1, it can be seen that the JWD is large, heavy and very expensive (US \$12,000). Its power consumption is also very high and its moving surface will require frequent maintenance. Due to these limitations, such a disdrometer cannot be used for remote locations and dense applications, as is required by TAHMO.

1.4.2 Optical Disdrometer

Another category of disdrometers is based on optics. An optical disdrometer uses a beam of infrared light to determine the size of a raindrop. As shown in Figure 1.5, an optical disdrometer continuously transmits a beam of infrared light from one side of the instrument and receives on the other side. When a raindrop passes the beam, the intensity of the light received at the other end reduces. The magnitude of the reduction is a function of the raindrop's size.

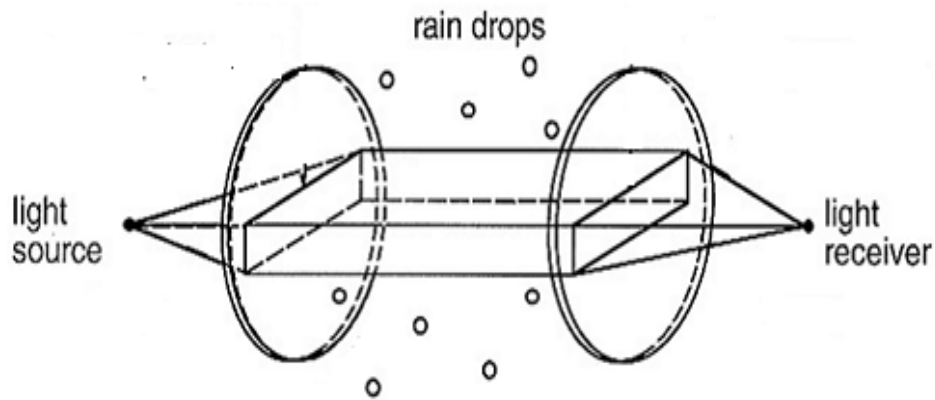


Figure 1.5 Schematic of optical disdrometer [8]

Thies Clima Laser Precipitation Monitor [9]

The Thies Clima's disdrometer is a Laser Precipitation Monitor (LPM) system that belongs to the category of optical disdrometers. Apart from the size of a raindrop, it can also determine the speed of a raindrop. As shown in Figure 1.6, an infrared light beam is continuously transmitted from one side of the disdrometer and received at the opposite. When a raindrop passes the beam, the infrared light gets scattered and the intensity of the light reduces at the receiver [9]. The reduction in intensity corresponds to the size of the raindrop.



Figure 1.6 Thies Clima laser precipitation monitor based on optical disdrometer principle [9]

The LPM has the following specifications (Table 1-2):

Table 1-2 Specifications for LPM disdrometer [9]

Parameters	
Range (along diameter)	0.16 mm to 8mm
Resolution	22 classes
Sampling Area	46 cm ²
Approx. Cost	US \$4,500
Weight	4.8 Kg
Dimensions	27 x 17 x 54 cm ³
Power	24 V AC /750 mA

The LPM requires less maintenance than the JWD. But, its size, weight, cost and power consumption are still high.

1.4.3 Acoustic Disdrometer

As shown in Figure 1.7, an acoustic disdrometer uses the sound generated by impinging raindrops on the sensor's surface. The principle behind an acoustic disdrometer is the same as that of an ordinary microphone in which a transducer converts sound waves into electrical signals. In an acoustic disdrometer, the strength of the sound wave depends on the size of the raindrops. By using an appropriate transduction method, the generated sound wave can be converted into an electrical signal. Now, the size of a raindrop can be measured by applying a calibrated transfer function to the electrical signal.

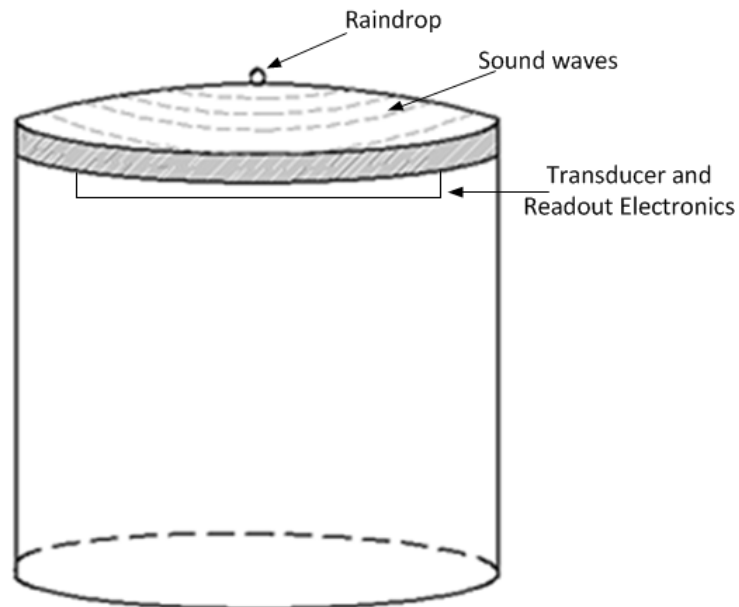


Figure 1.7 Schematic of acoustic disdrometer

Vaisala RainCap [10]

The Vaisala RainCap (VR) is based on the acoustic detection of the impact of a raindrop. Unlike the other disdrometers mentioned, the VR only provides information about the rainfall rate. But internally it does this by measuring the size of raindrops.

Figure 1.8 shows an image of a VR. It consists of a piezoelectric detector attached to the underside of a stainless steel cover. When a raindrop hits the cover, it generates an acoustic signal. The piezoelectric transducer converts the acoustic signal into a voltage pulse which is a function of raindrop size.



Figure 1.8 Vaisala RainCap disdrometer based on acoustic disdrometer principle [11]

The VR has the following specifications (Table1-3):

Table 1-3 Specifications of Vaisala RainCap [12]

Parameters	
Range (along diameter)	1 mm – 5 mm
Resolution	8 classes [10]
Sampling Area	60 cm ²
Approx. Cost	US \$2,500
Weight	0.65 Kg
Dimensions	N.A
Power	3mA @ 12VDC

Compared to the JWD and LPM, the VR weighs less and consumes less power. But, it is sold as a mini weather station which makes it very costly compared to the target cost of US \$200 for the complete weather station.

1.4.4 Summary

In the current section, various disdrometers have been discussed. Table 1-4 presents the summary of the discussion.

From the table it can be seen that all the presented disdrometers are very expensive compared to the target cost of the complete weather station (US \$200). The high cost of these disdrometers can be attributed to the technology involved. For example, in the LPM, a laser beam of a specific wavelength must be generated and received, which makes it an expensive instrument. In the case of the VR, the disdrometer is probably cheap but the total solution is expensive.

Table 1-4 Comparison of the presented disdrometers

Parameters	JWD	LPM	VR
Principle	Displacement	Optical	Acoustic
Range (raindrop size along diameter)	0.3 mm to 5 mm	0.16 mm to 8mm	1 mm to 5 mm
Resolution	127 classes	22 classes	8 classes
Sampling Area	50 cm ²	46 cm ²	60 cm ²
Approx. Cost	\$ 12,000	US \$4,500	US \$2,500
Weight	5.1Kg	4.8 Kg	0.65 Kg
Dimensions	10 x 10 x 17 cm ³ (Sensor Unit) 12 x 26 x 27 cm ³ (Processing Unit)	27 x 17 x 54 cm ³	N.A
Power	115/230 Volts AC, 5.5 VA, (9 to 18 Volts DC; 3.3 Watts, also possible)	24 V AC /750 mA	3mA @ 12VDC (Stand by)

Also, the presented disdrometers are bulky, consume a lot of power and require frequent maintenance, which makes them unsuitable for large scale (20,000 units), remote deployment.

These drawbacks motivate the need to develop a new kind of disdrometer which can also be used for various scientific as well as for commercial purposes. The new disdrometer should meet the specifications given in Table 1-5.

Table 1-5 Target specifications for a new disdrometer

Parameters	
Range (along diameter)	0.3 mm to 5.5 mm
Resolution	128 Classes
Sampling Area	< 50 cm ²
Approx. Cost	<US \$50
Weight	<100gms
Dimensions	< 5 x 5 x 7 cm ³
Power	<20mA @ 5 V

1.5 Low-Cost Disdrometer by DWM

In 2009, the Department of Water Management (DWM) at TU Delft conceptualized the design of a low-cost disdrometer which is suitable for large scale, remote deployment as is required by TAMHO. Figure 1.9 shows the current version of the proposed disdrometer [2]. It belongs to the category of acoustic disdrometers and weighs approximately 50gm. It uses a piezoelectric ceramic diaphragm as the transducer. The piezoelectric diaphragm converts the sound waves generated by the impact of a raindrop into electrical signal. In the current report, this disdrometer will be referred to as the DWM disdrometer.



Figure 1.9 DWM disdrometer [2]

Experiments were conducted with the DWM disdrometer and a proof of concept was delivered in [14]. A tipping bucket was used as the reference during the experiments. It was found that the rain rate measured by the DWM disdrometer is remarkably similar to that measured by the standard tipping bucket, at least during heavy rainfall.

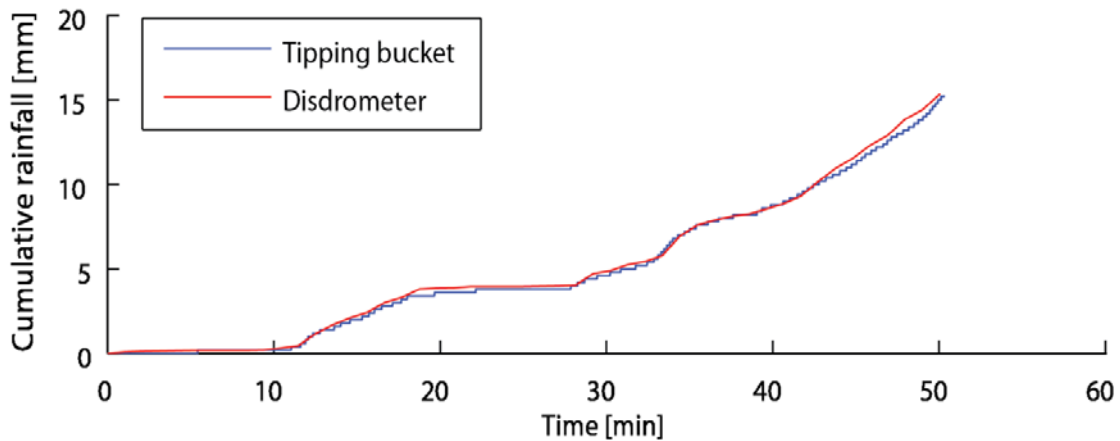


Figure 1.10 Comparing the calculated rainfall rate given by disdrometer with standard tipping bucket for heavy rainfall [13]

Figure 1.10 shows a result for one such rain event. The cumulative rainfall information calculated from the DWM disdrometer is in agreement with the output of tipping bucket.

On the contrary, measurements made by the disdrometer and the tipping bucket deviate significantly for less intense rain events. Figure 1.11 shows a measurement result for one such event. The result shows a large underestimation of rainfall rate by the disdrometer. This is because of the absence of small drops in the data collected by the DWM disdrometer [13].

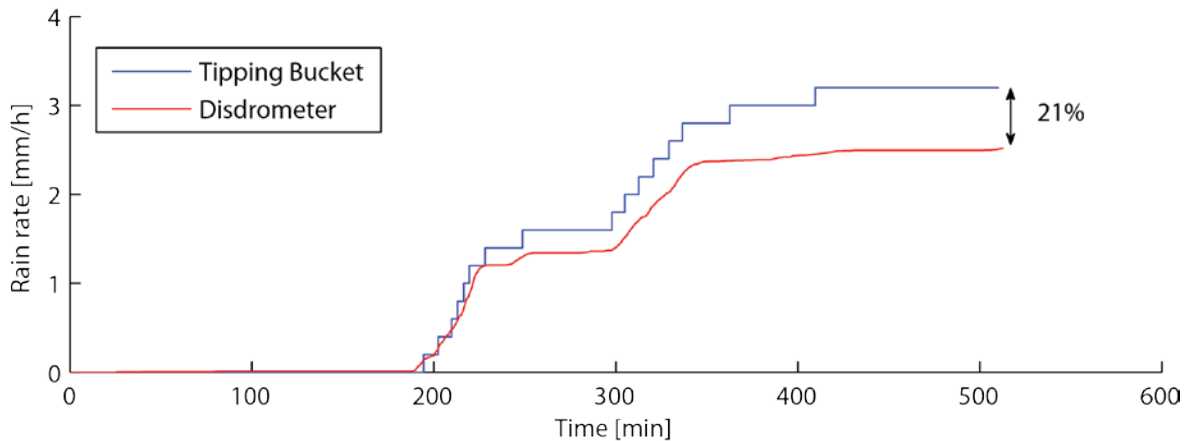


Figure 1.11 Comparing the calculated rainfall rate given by disdrometer with standard tipping bucket for light rainfall (< 5mm/hr) [13]

During a rain event, the size of a raindrop can vary from 0.1mm to 8mm in diameter. For less intense rain, most of the drops are smaller in size and vary between 0.1mm to 1mm along the diameter. A small raindrop generates a very low amplitude sound wave and requires a very sensitive transducer. So, the absence of small drops can be attributed to the poor sensitivity of the transducer or to the high intrinsic noise of the transducer and its readout circuit. Therefore, the transducer and its readout circuit needs to have high sensitivity and low-intrinsic noise in order to measure a small raindrop (<1mm along the diameter).

Also, if a raindrop hits the edge of the DWM disdrometer, only part of its kinetic energy is transferred to the transducer. Because of this, the DWM disdrometer underestimates the size of the raindrop and generates an error. This is known as the edge effect. The inaccuracy due to the edge effect can be reduced by increasing the catchment area of the disdrometer [2]. But a large catchment area increases the cost of the disdrometer and also the chance of multiple drop impacts. So, a method is required to filter out the edge drops, thus increasing the accuracy of the disdrometer, without a significant cost penalty.

The current project was initiated to address the aforementioned challenges. In the presented work, a characteristic model of the DWM disdrometer has been derived. Further, a transfer function relating the size of a raindrop to the sensor's output signal has been proposed and verified. Based on the model and the transfer function, a readout circuit for the DWM disdrometer has been designed. Also, an innovative technique has been proposed and verified to reduce the edge effect.

1.6 Thesis Organization

The remaining chapters of this report are organized as follow:

Chapter 2 introduces the specifications associated with a raindrop and a rain event. A discussion of the formation, shape and size of a raindrop is given at the beginning of the chapter. It is followed by a discussion on the terminal velocity and momentum of a raindrop. The Drop Size Distribution (DSD) during a rain event and its applications are discussed next. Furthermore, the chapter explains the piezoelectric effect which is followed by a discussion of the piezoelectric material used and its associated parameters.

Chapter 3 gives a brief description of the DWM disdrometer, its transducer and its packaging. This is followed by a discussion of the equivalent electric circuit model of the DWM disdrometer. Later, an empirically derived transfer function between the raindrop momentum and the disdrometer's output signal is presented. Furthermore, issues such as accumulation of water on the disdrometer surface (puddling effect), and wrong interpretation of data when a rain drop hits on the edge of the disdrometer (edge effect) have been explained and their solutions are proposed and verified.

Chapter 4 derives various electrical specifications, like dynamic range, bandwidth, noise and power, of the readout circuit of the DWM disdrometer. Based on these specifications, a readout circuit design has been proposed and designed on PCB. Various measurement results obtained from the designed readout circuit and the DWM disdrometer are also presented in the chapter.

Chapter 5 presents the important conclusions drawn from the research conducted in the presented work. The chapter also gives a few recommendations for topics which deserve to be subject of further study.

Chapter 2 Measurand and Transducers

The characteristics of the measurand and the transduction principle of the disdrometer need to be understood before embarking on the design of a readout circuit. A raindrop is the measurand of a disdrometer. First of all, the drop formation process is discussed, as this defines the shape and size of a raindrop. It will be followed by a discussion of the terminal velocity and the momentum of a raindrop. Section 2.2 explains the piezoelectric effect and how a piezoelectric element can be used to measure the size of a raindrop.

2.1 Raindrop Characteristic

A raindrop is the measurand of a disdrometer. So, it is important to understand the parameters governing its shape and velocity profile. A raindrop, before impinging on the disdrometer, goes through a number of coalescence and disintegration cycles. These phenomena not only affect its shape but also change its velocity [14]. This section will present a brief introduction to different properties of a raindrop such as its size, terminal velocity and momentum.

2.1.1 Formation of Raindrops

The actual process of raindrop formation is very complex and a complete description is out of this work. But to understand the measurand of the disdrometer, a very brief description of the raindrop formation process will be provided in the following.

Raindrops are formed from the water that is always present in the atmosphere. Generally, air is warmer near the earth's surface and thus, water remains in vaporized state. As the altitude increases, the temperature of the air decreases and water vapour starts to condense, forming water droplets. These droplets remain stationary in the atmosphere and do not fall due to air resistance. During air turbulence, water droplets collide and coalescence takes place to produce drops. At some point a drop becomes heavy enough to overcome the air resistance and starts falling as a raindrop. Coalescence of raindrops continues even during the descent. When a drop grows sufficiently large, it disintegrates to form multiple small drops. This process of coalescence and disintegration continues until the raindrop hits the ground.

2.1.2 Shape and Size of Raindrop

Raindrops are roughly spherical or oblate spheroids in shape [15], and are quite unlike teardrops. As shown in Figure 2.1.a, small raindrops are spherical in shape, while larger drops become flattened on the bottom, like hamburger buns, due to air resistance. Generally, an equivolume diameter is used to characterize the size of a raindrop. As demonstrated in Figure 2.1.b, the equivolume diameter of a raindrop is defined as the diameter of a perfect sphere of the same volume as the raindrop [15]. Raindrops typically have sizes ranging from 0.1mm to 8mm in

equivalent diameter. Beyond about 8mm of equivalent diameter, raindrops break up into smaller drops.

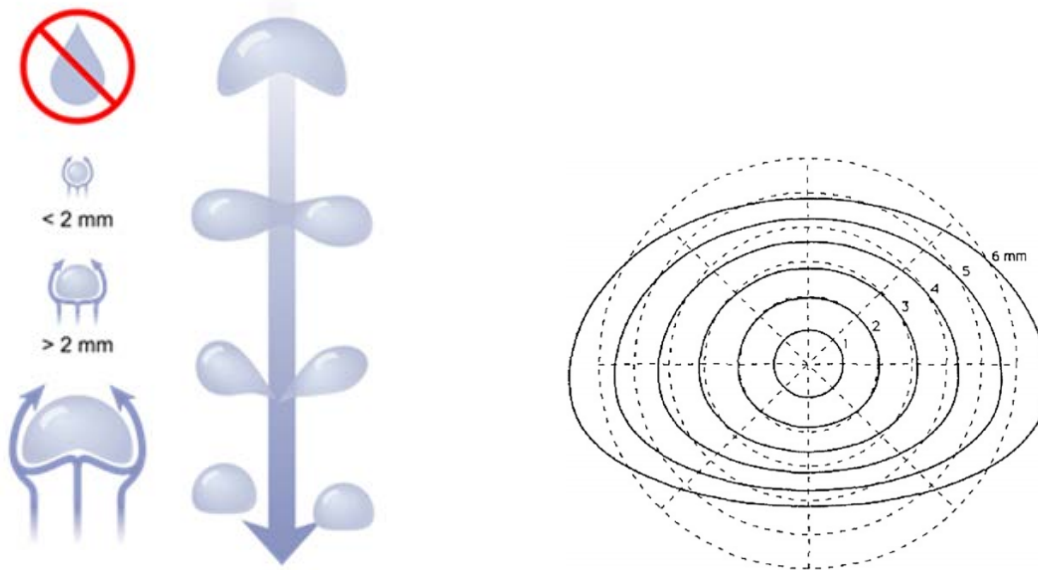


Figure 2.1 (a) Shapes of raindrops [16], (b) equivalent diameter of raindrops [15]

2.1.3 Terminal velocity

Two opposite forces, air drag and gravitational force, act on a falling raindrop. A raindrop accelerates towards the earth's surface under the influence of gravity. As its velocity increases, the drag force on the raindrop, caused by air resistance, also increases. When the drag force becomes equal to the gravitation force, the net acceleration of the drop becomes zero. Under this zero acceleration condition, the raindrop falls at a constant velocity known as terminal velocity. A bigger raindrop needs approximately 12 meters of free fall before it attains terminal velocity, whereas small drops can attain terminal velocity from much smaller heights [17]. This implies that a raindrop attains its terminal velocity well before it reaches the earth surface.

The terminal velocity of a raindrop is proportional to its size [17]. A number of field experiments have been performed to measure the terminal velocity of raindrops [18, 19, 20]. The most popular and definitive data for raindrop terminal velocities is provided by [19]. This empirically derived data spans raindrop diameters ranging from 0.1mm to 5.8 mm. A power law relationship (eq.(2.1)) between the diameter of a drop and its terminal velocity can be used to fit the [19] data into one equation [2].

$$v(D) = \alpha D^{\beta} \quad (2.1)$$

Where, 'D' is the raindrop diameter, $\beta = 0.67$ and $\alpha = 3.778 \text{ ms}^{-1}\text{mm}^{-\beta}$ are empirically derived constants using the data of [19]. The values of α and β provide a close fit in the range of 0.5mm

$\leq D \leq 5.0$ mm [2]. In this report, eq. (2.1) is used as the basis for computing the terminal velocity of a raindrop.

2.1.4 Momentum of a raindrop

Momentum is a physical quantity associated to an object and is a measure of its motion. At any instant, all objects possess momentum irrespective of their state of motion. The momentum of an object is given as the product of its mass and velocity:

$$M_0 = m_0 v_0 \quad (2.2)$$

where, M_0 is the momentum, m_0 is the mass and v_0 is the velocity of the object.

When a raindrop starts falling, it gains velocity and thus momentum. At terminal velocity, a raindrop reaches its maximum vertical momentum and maintains it until the drop hits any surface. Due to momentum conservation, the raindrop transfers all its momentum to the colliding surface, to a first order approximation.

For a raindrop with equivolume diameter ' D ', the mass m_0 of the raindrop is given by

$$m_0 = \frac{\rho \pi D^3}{6} \quad (2.3)$$

where, $\rho = 1 \text{ gm/mm}^3$ is the density of a raindrop.

So, for a raindrop, both its mass and terminal velocity are functions of its equivolume diameter. Thus, a direct relationship exists between the momentum of a raindrop and its equivalent diameter. The relation is given by:

$$M_0 = m_0 v_0 = \frac{\rho \pi D^3}{6} \alpha D^\beta = \frac{\alpha \rho \pi D^{3+\beta}}{6} \quad (2.4)$$

In the next chapter, the momentum of a raindrop given by(2.4) will be used to derive a transfer function between ' D ' and the output signal of a disdrometer.

2.1.5 Drop Size Distribution (DSD)

As explained in Section 2.1.1, formation of a raindrop during rainfall is a complex process. Collision, coalescence and disintegration of raindrops result in an array of raindrop sizes which is not fixed but is distributed over a range of equivalent diameters. The volumetric distribution of drops, $N(D)$, is defined as the Drop Size Distribution (DSD) i.e. $N(D)dD$ is the number of drops per unit volume in the diameter range D to $D+dD$. Figure 1.1 shows an example of a DSD.

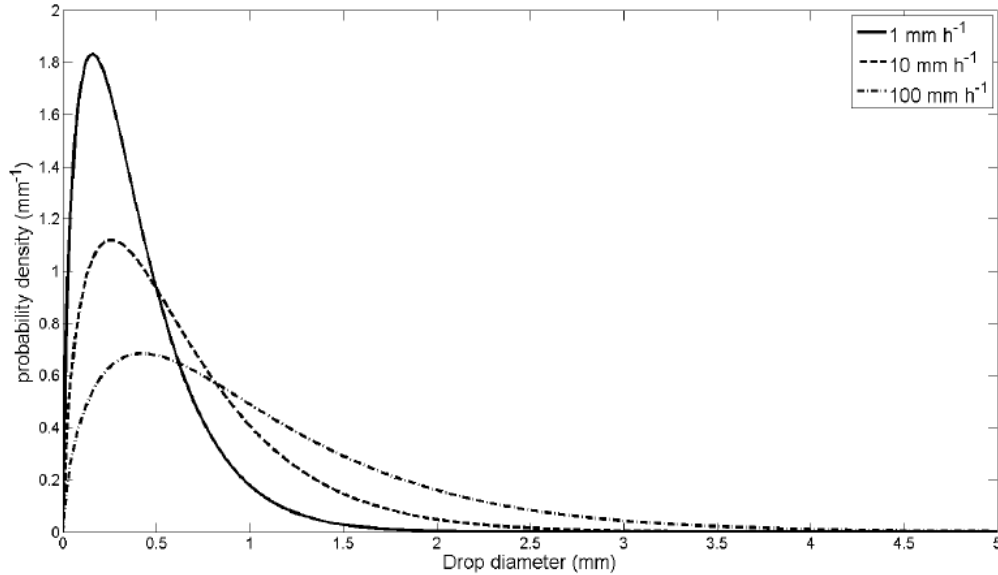


Figure 2.2 Drop Size Distribution for raindrops during rainfall [21]

The DSD for a rain event depends on the rain intensity [21]. Figure 2.2 shows the probability distribution of raindrop size for three different rain intensities. From the figure it is clear that during low intensity rain (1mm/hr) most of the raindrops will be small in size. But during heavy rainfall, the probability of having bigger drops increases significantly.

As mentioned in Section 1.2, several parameters that are of interest for applications like microwave communication and soil erosion can be derived from the moments of DSD [22]. The n^{th} moment of DSD can be defined as

$$M_n = k \int_0^{\infty} D^n N(D) dD \quad (2.5)$$

where, k is the constant of proportionality.

Some of the important parameters which are proportional to the integer moments of DSDs are:

1. $n = 0$: total number of drops
2. $n = 3$: water volume per unit atmosphere volume
3. $n = 4$: rainfall intensity (approximate)
4. $n = 5$: kinetic energy flux density (approximate)
5. $n = 6$: radar reflectivity and specific attenuation (in Rayleigh region)

2.2 Transduction Principle

The disdrometer used in this project makes use of a piezoelectric disk as the transducer. As piezoelectric disks are made of ceramic, the piezoelectric properties of ceramic and the corresponding constants and coefficients are discussed next.

2.2.1 The Piezoelectric Effect

Any material that develops an electric charge or polarity on the application of an external mechanical stress, or vice versa is known as a piezoelectric material. The phenomenon of generation of electrical charges in response to an external mechanical stress is known as the direct piezoelectric effect. Conversely, the phenomenon in which mechanical deformation occurs due to the application of an electric field is known as the reverse, or indirect, piezoelectric effect. Lead Zirconate Titanate (PZT) and Quartz are the two most popular examples of piezoelectric materials. They are frequently used in the medical, aerospace and nuclear instrumentation.

Figure 2.3 illustrates both the direct and indirect piezoelectric effect. Figure 2.3.a shows the poling axis in a piezoelectric material. The poling axis of a piezoelectric material determines the polarity of the material under stress. The axis is defined during a polarization step during the manufacture of the material.

As shown in Figure 2.3.b, if the material is compressed, a voltage of the same polarity (as the poling axis) appears between the electrodes. If stretched, a voltage of opposite polarity appears (see Figure 2.3.c). Conversely, if a voltage is applied, the piezoelectric material will deform. A voltage with opposite polarity as the poling axis will cause the material to expand (shown in Figure 2.3.d). A voltage with the same polarity will cause the material to compress, as depicted in Figure 2.3.e. If an AC signal is applied, as shown in Figure 2.3.f, the material will vibrate at the same frequency as the signal.

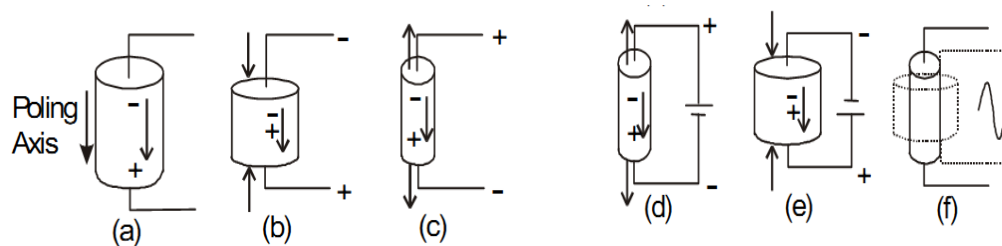


Figure 2.3 Example of piezoelectric effect [23]

The piezoelectric materials available in the market can be classified into two classes: crystal and ceramic. The current research focuses only on ceramic materials and their properties will be explained next.

2.2.2 Piezoelectric Ceramics

Ceramic is an artificial piezoelectric material. It is a preferred piezoelectric material because of the ease with which it can be manufactured into a variety of shapes and sizes. The most commonly produced piezoelectric ceramics are PZT, Barium Titanate and Lead Titanate.

The basic principle behind the piezoelectric property of a ceramic can be understood by a molecular level inspection. Typically, ceramic materials have ionic bonding and are polarized, i.e. one end of a molecule is negatively charged, while the other end is positively charged. This forms an electric dipole. In the absence of external force, as depicted in Figure 2.4.a, the dipoles formed by the molecules cancel each other due to the symmetry of the structure, and no electric

field is observed. But under stress (see Figure 2.4.b), the material deforms and loses its symmetry, resulting in the creation of a dipole moment. This dipole moment forms an electric field across the material and hence a voltage appears.

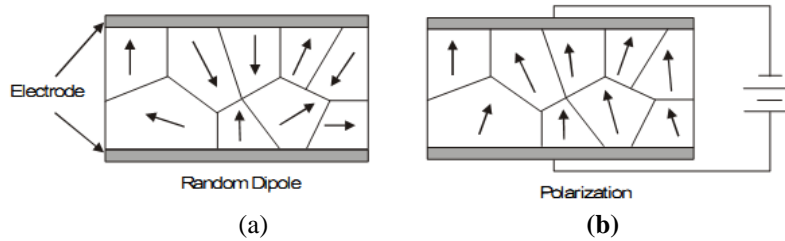


Figure 2.4 Polarization of ceramic material [23]

Material parameters [24]

Various coefficients and parameters associated with ceramic materials are given in this section. It is important to realize that the material properties of a piezoelectric element depend on the orientation of the applied energy (mechanical/electrical) along the poling axis. Therefore, it is essential to maintain a constant axis numbering scheme. Conventionally, a tensor notation (as shown in Figure 2.5) is used to identify the direction in a piezoelectric material.

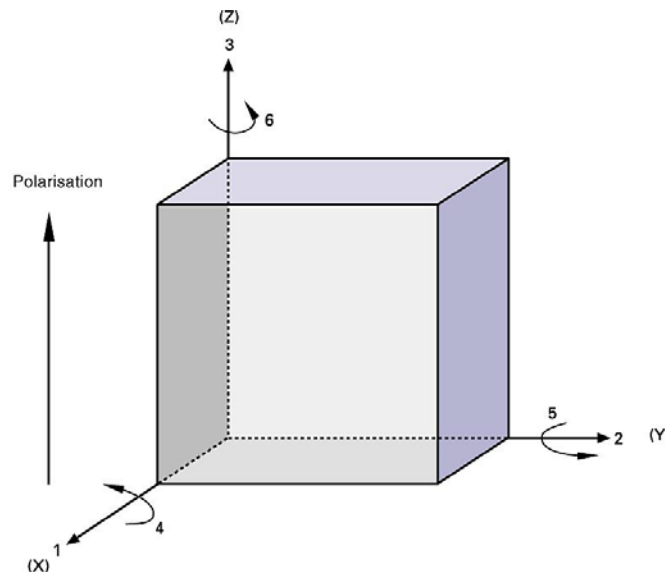


Figure 2.5 Tensor notations for piezoceramic material [2]

The polar, or axis 3, is considered to be parallel to the direction of polarization within the ceramic, with axes 1 and 2 perpendicular to it. The terms 4, 5 and 6 refer to shear strains associated with the 1, 2 and 3 directions, respectively.

All the coefficients and parameters, to be explained, have double subscripts linked to the electrical and mechanical quantities associated with the material. The first subscript gives the

direction of the electric field associated with the voltage applied or the charge produced. The second subscript gives the direction of the mechanical stress or strain. For example, the d_{33} coefficient is associated with the electric field applied in the poling axis direction and mechanical deformation in the same direction. These coefficients and parameters are used later in this report.

1. *Resonant (f_r) and anti-resonant (f_a) frequency*: Similar to any solid object, a piezoceramic element also has certain characteristic frequencies at which it resonates preferably. When excited at this frequency, ' f_r ', the element resonates freely with large amplitude than that at other frequencies. Whereas, at anti-resonant frequency ' f_a ' the impedance of the element is at a maximum and the oscillation amplitude is at minimum.

2. *Piezoelectric charge constant (d-coefficient)*: The piezoelectric constants relating the mechanical strains produced by application of electric fields are termed as the charge constants, or "d" coefficients. Conversely, the coefficients can be seen as a relation between the charges collected on the electrodes and the applied mechanical stress.

$$d_{ij} = \frac{\text{Strain Development}}{\text{Applied Electric field}} \quad (2.6)$$

where, ' i ' and ' j ' define the direction of electric field and mechanical stress, respectively. Large values of d-coefficients are required for any material to be used as an actuator.

3. *Piezoelectric voltage constant (g-coefficient)*: The piezoelectric constants, relating the electric field produced by a mechanical stress, are termed as the voltage constants or the "g" coefficients.

$$g_{ij} = \frac{\text{Open circuit Electric field}}{\text{Applied Mechanical Stress}} \quad (2.7)$$

High values of g-coefficients are desirable for materials intended to be used as sensors. Also, there exists a relation between the g-coefficients, and the d-coefficients:

$$d_{ij} = \epsilon_{ij}^T g_{ij} \quad (2.8)$$

where, ϵ_{ij}^T is the dielectric constant of the material measured under the application of a constant stress.

4. *Piezoelectric coupling coefficient (k-coefficient)*: This is a measure of the overall strength of the electromechanical effect. It describes the conversion of energy by the ceramic element, from mechanical to electrical form or vice versa.

$$k_{ij} = \sqrt{\frac{\text{Electrical Energy Stored}}{\text{Mechanical Energy Applied}}} \quad (2.9)$$

The value of ' k_{ij} ' is always less than unity because the transfer of energy from one form to another is never 100% efficient. For a thin disc, like piezoelectric diaphragm, the coupling coefficient is approximately given by:

$$k_{ij} \approx \frac{f_a^2 - f_r^2}{f_r^2} \quad (2.10)$$

5. *Dielectric Constant (K)*: The relative dielectric constant is the ratio of the permittivity of the material, ϵ , to the permittivity of free space, ϵ_0 , in the unconstrained condition, i.e., well below the mechanical resonance of the part.

$$K = \frac{\epsilon}{\epsilon_0} \quad (2.11)$$

At resonance, the dielectric constant will be reduced by the factor $(1 - k_{ij}^2)$, where ' k ' is the coupling coefficient.

6. *Capacitance(C)*: The capacitance of a material is defined as the product of its relative dielectric constant (K) by the permittivity of free space ($\epsilon_0 = 8.9 \times 10^{-12}$ farads/meter) and electrode surface area (A), divided by the thickness (t) separating the electrodes. Therefore, it depends on the type of material and its dimensions.

$$C = \frac{K\epsilon_0 A}{t} \quad (2.12)$$

7. *Elastic Compliance (s)*: This is the ratio of the material's change in dimensions (strain) in relation to an externally applied load (stress). In other words, it is the inverse of Young's modulus and can be calculated using the eq (2.13) and (2.14).

$$s_{33}^D = \frac{1}{4\rho f_a^2 l^2} \quad (2.13)$$

$$s_{33}^E = \frac{s_{33}^D}{(1 - k_{33}^2)} \quad (2.14)$$

where, l is the distance between electrodes. The superscripts D and E stand for constant electric displacement (open circuit) and constant electric field (short circuit) respectively.

All the aforementioned parameters and coefficients depend on the material's composition. It is, therefore, possible to tune the value of these properties by various methods. One way to do this is through adding dopants to the ceramic formulation.

2.3 Conclusion

This chapter described raindrop characteristics such as formation process, size and velocity. Furthermore, the Drop Size Distribution (DSD) of a rain event was discussed. It was also explained that the moments of DSD can be used for various applications such as prediction of soil erosion and radar reflectivity. Finally, the chapter concludes with a discussion on the transduction principle of piezoelectricity and the parameters associated with piezoceramic materials.

Chapter 3 Sensor Modeling and Characterization

In this chapter, the DWM disdrometer and its transducer are described in Section 3.1. The selection criterion for the transducer is also discussed. In Section 3.2, the electrical modeling of the disdrometer is described. The equivalent electric circuit model for the DWM disdrometer is derived and verified by simulation results. The generation of output signal by the disdrometer is analyzed and verified in Section 3.3. Based on the results obtained from Section 3.3, a relationship between the raindrop size and the output signal is deduced in Section 3.4. In Section 3.5, the edge effect, which is a source of error for the disdrometer is discussed. A solution for this problem is proposed and verified by the experiments.

3.1 Proposed Sensor System

In 2009, Degen [26] proposed a new low-cost disdrometer (Figure 3.1.a) using an ordinary piezoelectric diaphragm (PED). It was based on the acoustic disdrometer principle and used an audio recorder to acquire signals from the transducer. Its proper operation was verified by various experiments. But, several issues such as rusting of the sensor element, large amount of output data to store (several gigabytes) and low resolution were also observed.

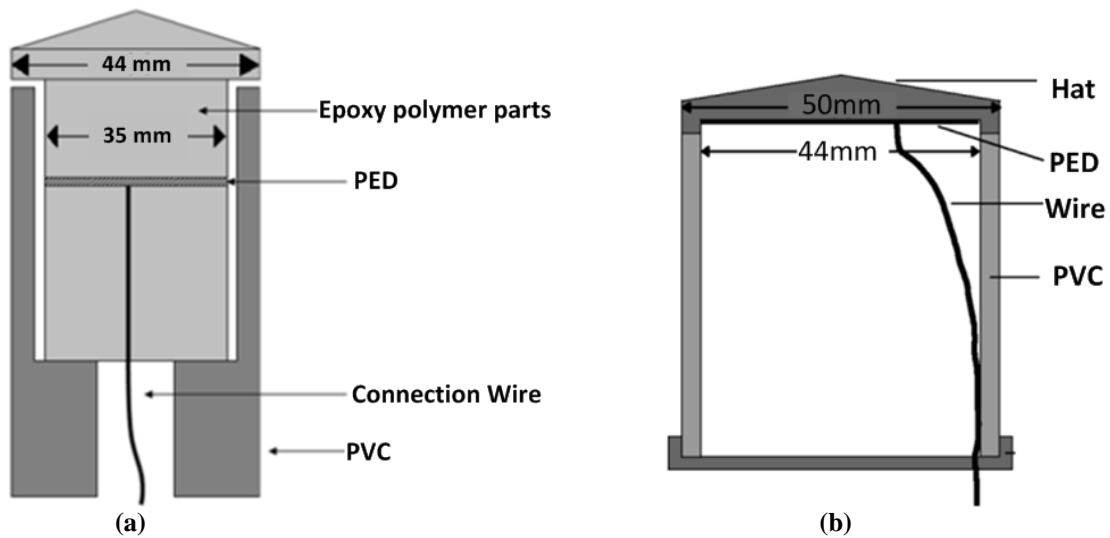


Figure 3.1 Schematic of prototypes: (a) designed by Degen, (b) designed by Stijn [2]

Later, Stijn [2] improved Degen's design and developed a prototype of the disdrometer presented in Figure 1.8. Figure 3.1.b shows the schematic of the prototype developed by Stijn. There are three important parts of this prototype: the PED, a PVC casing and a plastic cover or "hat". For the current research work, only the PED and the hat of the sensor are of interest. In order to

develop an equivalent circuit model and to define the specifications for the readout circuit, the prototype developed in [2] has been used.

3.1.1 Hat of the sensor

As shown in Figure 3.1, the top surface of the DWM disdrometer is referred to as the hat. Because of its low cost and water repellent properties, the hat is made from polyvinyl chloride (PVC) [2]. Also, it is easy to make a water-tight junction between two PVC pieces with glue. As shown in Figure 3.2.a, the hat is designed to have a conical shape to prevent accumulation of water on the sensor surface and has a diameter of 50mm. On the flip side, it has one flat surface as shown in Figure 3.2.b with an internal diameter of 44mm, equal to the size of the PED. The PED is glued to the hat as shown in Figure 3.2.c.

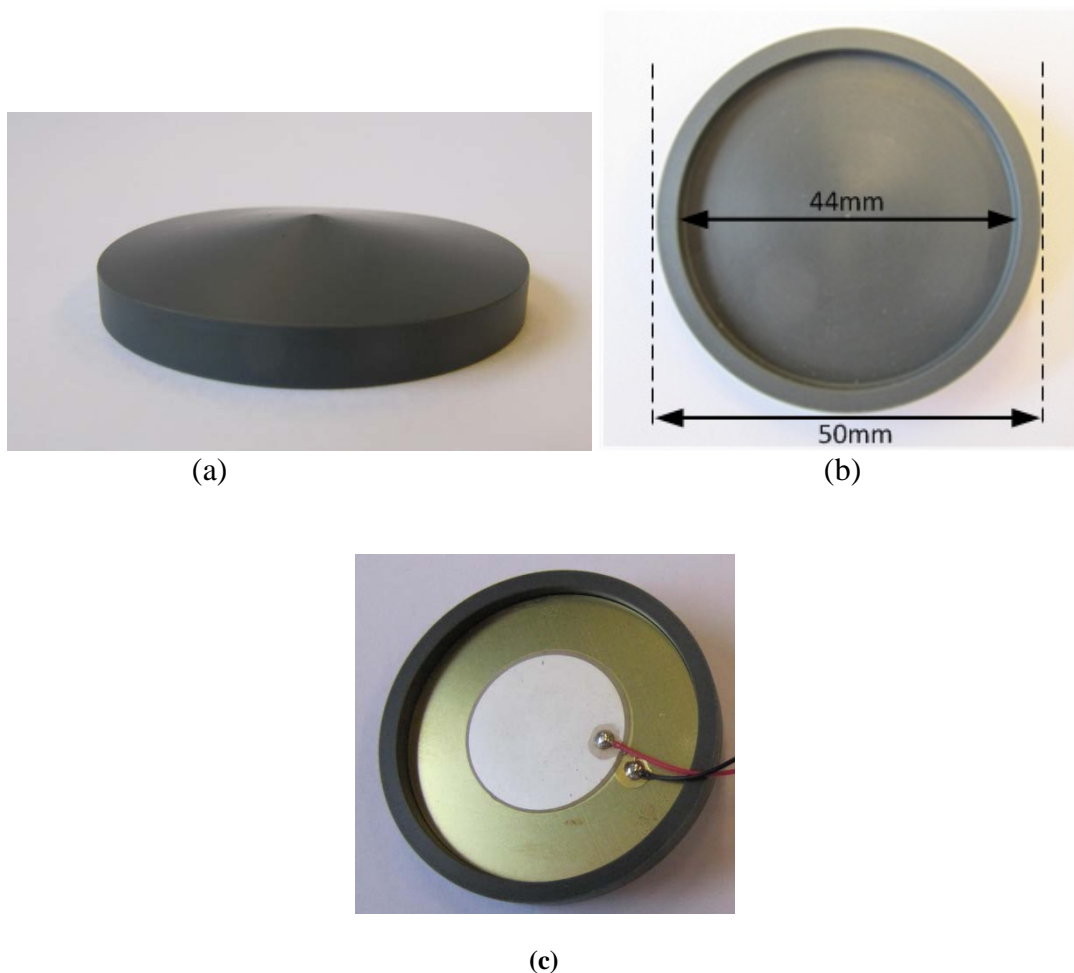


Figure 3.2 Hat of the disdrometer: (a) side view, (b) bottom view, (c) with PED

Puddle Effect

Even with a conical shape, contrary to expectations, it was observed that water accumulates on the hat. As shown in Figure 3.3, it accumulates mainly on the edges of the hat. This effect is

primarily observed during drizzling. In the case of heavy rain, a big drop impinging on the surface spills out most of the accumulated water.



Figure 3.3 Puddle effect: accumulation of water on the hat of the disdrometer

This accumulation occurs due to the sharp edges of the hat and the surface tension of water. A novel hat, containing smooth outer edges, is proposed to resolve the mentioned issue. It has been observed that the new design causes significant reduction in the amount of accumulated water as shown in Figure 3.4.b.



(a)



(b)

Figure 3.4 Puddle effect on new hat (a) new hat with soft edge, (b) puddle effect on new hat

3.1.2 Piezoelectric Diaphragm

The Piezoelectric Diaphragm (PED) used as the transducer for the DWM disdrometer is shown in Figure 3.5.a. As shown in Figure 3.5.b, the PED consists of a piezoelectric ceramic layer with electrodes on both sides. One of the electrodes is glued to a metal plate with conductive adhesive. The metal plate also provides mechanical support to the ceramic layer.

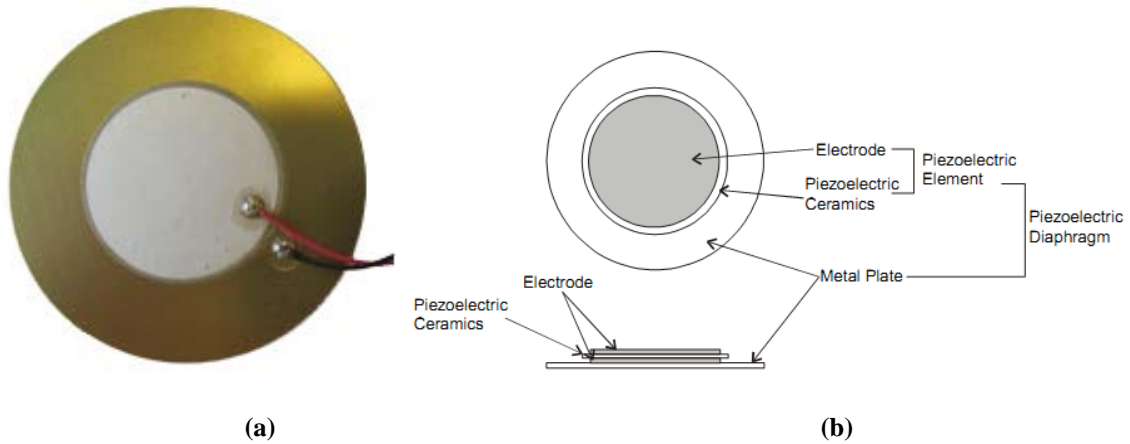


Figure 3.5 Piezoelectric diaphragm (a) PED used by Stijn [2] (b) construction of a PED [48]

PED Selection

Prior to this work, the criterion for selecting a PED for the DWM disdrometer application was solely based on the desired catchment area [2]. This is a tradeoff between the edge effect (explained in Section 3.5) and the probability of multiple drops hitting the sensor surface simultaneously. The edge effect is less for a disdrometer with a large catchment area [13]. But, the probability of simultaneous drop impact is higher on a large surface, leading to a wrong interpretation of the signal.

In the current section, a selection criteria based on the PED's specifications is derived. The criterion is based on the resonance frequency, thickness and area of the PED. The derivation of the selection criteria for PED is as follows:

In Section 3.2, it is shown that the electrical equivalent of a piezoelectric material is basically a capacitor. So, the output voltage, ' U_0 ' for a PED is given by:

$$U_0 = \frac{Q}{C} \quad (3.1)$$

where, ' Q ' is the charge generated on the ceramic due to the mechanical deformation and ' C ' is the capacitance of the disk.

The capacitance of the piezo-ceramic disk is given by eq. (2.12)

$$C = \frac{A(K\epsilon_0)}{t} \quad (3.2)$$

By equations (3.1) and (3.2):

$$U_0 = \frac{Qt}{A(\epsilon_0 K_3^T)} \quad (3.3)$$

where, the subscript '3' denotes the dielectric constant in the direction of the poling axis and the superscript 'T' denotes the dielectric constant under constant stress.

Using the definition of piezoelectric charge constant given in Eq. (2.6), eq. (3.3) can be written as:

$$U_0 = d_{33} \frac{Ft}{A(\epsilon_0 K_3^T)} \quad (3.4)$$

As given in [24], the piezoelectric charge coefficient can also be computed from the coupling coefficient, elastic coefficients and the dielectric constant. The relation is given by:

$$d_{33} = k_{33} \sqrt{\epsilon_0 K_3^T s_{33}^E} \quad (3.5)$$

Using the eq (3.5), eq (3.4) can be re written as

$$U_0 = k_{33} \frac{Ft}{A} \sqrt{\frac{s_{33}^E}{\epsilon_0 K_3^T}} \quad (3.6)$$

Solving and simplifying the above equation using eq. (2.10) and eq. (2.12) gives

$$U_0 = \frac{F}{A} \sqrt{\frac{A}{Ct}} \frac{f_a^2 - f_r^2}{f_r^2} \frac{f_r^2}{t f_a^3 f_r \sqrt{8\rho}} \quad (3.7)$$

$$U_0 = \frac{F}{\sqrt{ACt^3}} \frac{f_a^2 - f_r^2}{f_a^3 f_r \sqrt{8\rho}} \quad (3.8)$$

From eq. (3.8) it can be seen that the output voltage of a ceramic PED is an inverse function of the following parameters:

1. Area of the diaphragm
2. Thickness of the ceramic disk
3. Resonance and anti-resonance frequencies of the diaphragm

Therefore in order to obtain a higher output voltage, a PED with small area, low resonance frequency and a thinner disk should be used. Using these criteria, an appropriate, commercially available PED can be selected for the DWM disdrometer.

3.2 Transducer Modeling

The PED shown in Figure 3.5.a has been used as the transducer for a low-cost DWM disdrometer. The general characteristics of the PED can be found from its datasheet. But the electrical characteristics of the complete packaged system are unknown. In order to characterize the system and to make an efficient readout circuit, it is necessary to treat the disdrometer as a part of the circuit. Thus, an equivalent electrical circuit model of the disdrometer, preferably using lumped components, is required.

In the current section, the impedance of the PED is presented and compared to the response of the packaged system. It is shown that packaging drastically changes the PED's impedance response. Therefore, a model is developed for the complete packaged disdrometer.

3.2.1 Impedance Characteristics of PED

To determine the equivalent electric circuit of a system, it is of prime importance to obtain its impedance response over a frequency range which can be translated into lumped components circuit. To investigate this for the given PED, it was connected to Agilent HP 4194A Impedance/Gain-Phase Analyzer. The impedance analyzer applies an input voltage to the PED and measures the resulting current to derive the PED's impedance over the specified frequency range.

The voltage level in the impedance analyzer is set to be 100 mV. The sweep frequency ranges from 100 Hz to 10 kHz. The response curves of the impedance value and phase of the given PED are as shown in Figure 3.6. From this impedance phase response, it can be seen that the values of the impedance phase lie between -77° to -90° , except in the neighborhood of the resonance near 2 kHz. This means that the specimen behaves like a capacitor in the absence of any resonance. This conclusion is also confirmed by a high value of impedance of the PED at low frequencies.

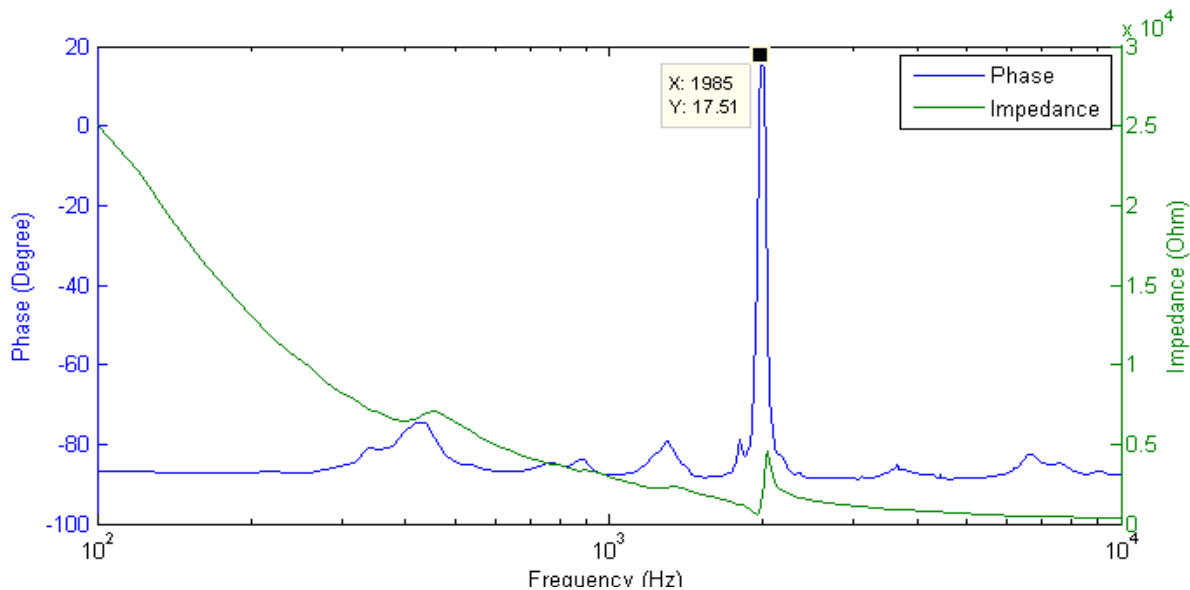


Figure 3.6 Impedance response of the given PED over a frequency range of 100Hz - 10KHz

3.2.2 Impedance characteristic of packaged PED

As was mentioned in Section 3.1, a PVC casing is used for the DWM disdrometer packaging. Due to the electromechanical coupling nature of the piezoelectric materials, the packaging (including glue used to attach PED on hat) greatly affects the electrical impedance characteristic of the PED.

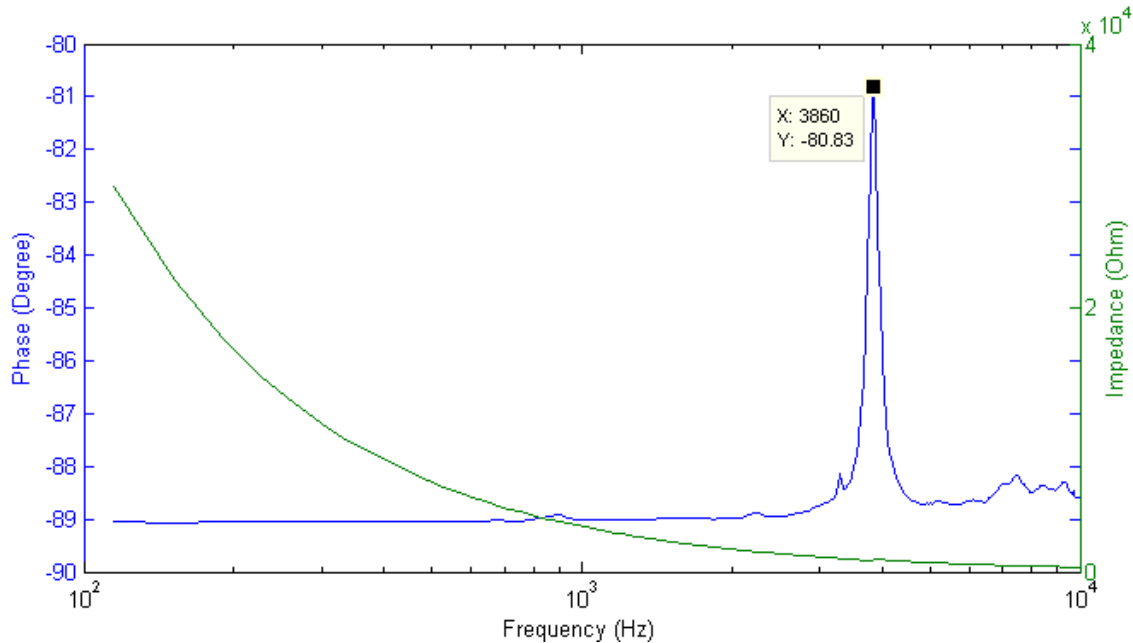


Figure 3.7 Impedance response of the given disdrometer over a frequency range of 100Hz – 10kHz

Figure 3.7 shows the impedance response of the packaged sensor with a new resonance frequency at 3.86 kHz. It can be observed that the resonance frequency got shifted higher. If a spring-mass system is used to model the damping oscillation of the PED [27], the resonance frequency will be given by:

$$f_r = \sqrt{\frac{k}{m}} \quad (3.9)$$

where, ' k ' is the effective spring constant and ' m ' is effective mass of the system.

An increase in the resonance frequency means that either the effective mass of the system has been reduced or that the effective spring constant has been increased. The potential reason for such a phenomenon is the series combination of PVC, glue and the PED itself. Analyzing this phenomenon will be complex, as the material properties are not known, and out of the scope of the current work.

So, the electrical equivalent circuit model is derived for the complete DWM disdrometer instead of only the PED element.

3.2.3 Equivalent Electric circuit Model

As shown in Figure 3.8, the frequency response of the disdrometer can be divided into two parts: (1) low frequency and non-resonant part; (2) high frequency and resonant part. The non-resonant part covers the frequency range of 100 Hz to 3.5 kHz and the resonant part cover the frequency ranging from 3.5 kHz to 6 kHz. Such breakup of frequency response of the disdrometer makes the process of modeling simpler and easy to understand. In the current section, both parts are explained and modeled separately. Finally, both the models are merged for developing the complete model of the transducer.

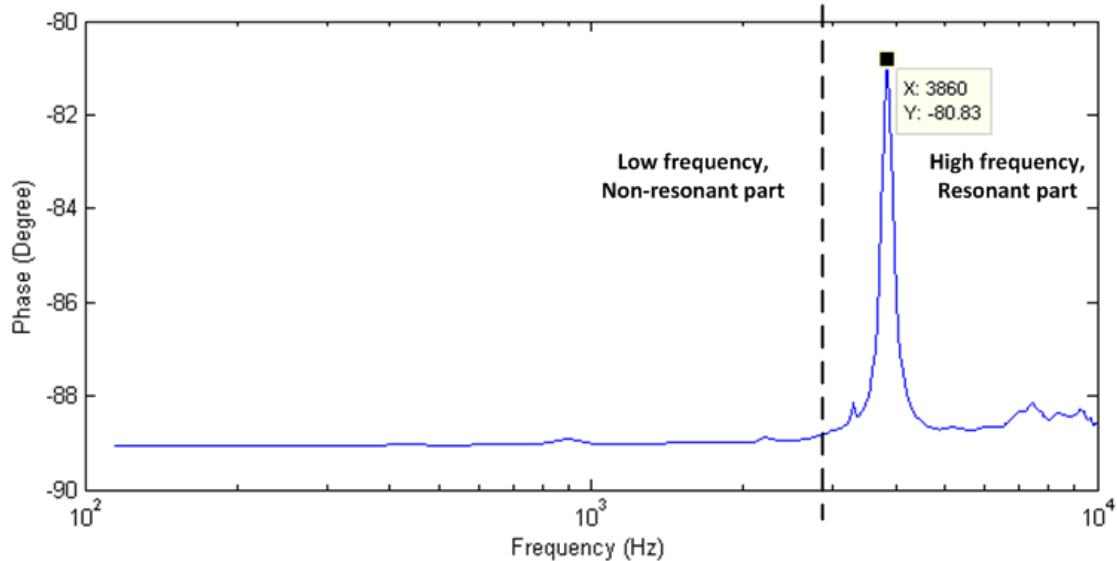


Figure 3.8 Partition of phase response of the given disdrometer into low frequency non-resonant part and high frequency resonant part over a frequency range of 100Hz - 10KHz

Model for the Resonant Frequency Part

The resonance frequency of a body can be defined as the frequency at which, when excited, the amplitude of vibration is much greater than that at other frequencies. From the electrical point of view, the resonance frequency of the piezoelectric transducer is where most of the power is concentrated in the power spectrum.

Figure 3.9 shows the equivalent circuit model of a piezoelectric element at resonance. This circuit is commonly referred as Van Dyke's Model and is recommended by the IEEE Standard on Piezoelectricity [28].

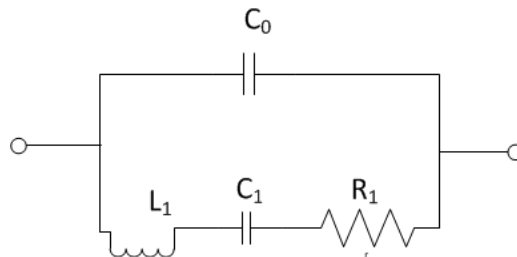


Figure 3.9 Van Dyke's model for a piezoelectric element at resonance[28]

Here, C_0 is the capacitance of the device in the absence of any mechanical deformation. The components L_1 , C_1 , R_1 are mass, elastic compliance and mechanical damping, respectively, transformed into electrical magnitude by the reverse piezoelectric effect. A detailed analysis of the Van Dyke's model can be found in [28]

Model for the Non-resonant Frequency

For the non-resonant part of the impedance characteristic several equivalent models [29, 30, 31, 32] have been proposed. But most of the proposed models are complicated and difficult to be applied in the real systems. The simplest model is one proposed by Guan [33]. Figure 3.10 shows the model proposed by Guan for the non-resonant part of the frequency.

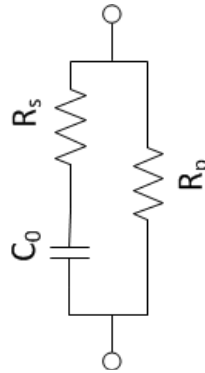


Figure 3.10 Model proposed by Guan for the non-resonant part of the frequency[33]

In this model, the capacitor C_0 represents the capacitance of the device. Component R_p is responsible for the internal charge leakage and R_s is associated with the energy dissipation.

Model for complete frequency response

A complete model of DWM disdrometer is given by combining both the resonant and the non-resonant equivalent electric circuit. The model shown in Figure 3.11 represents the complete impedance response of the DWM disdrometer.

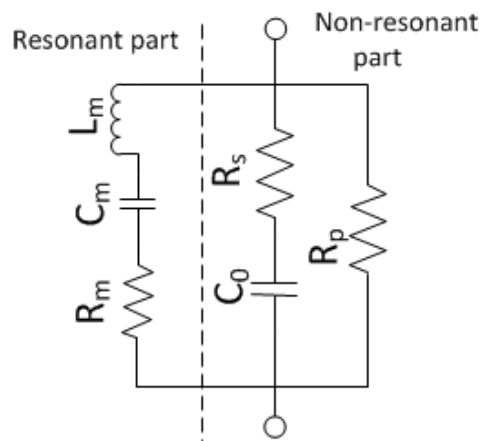


Figure 3.11 Equivalent model of the disdrometer [33]

Simulation and results

The model shown in Figure 3.11 has been used to characterize the given DWM disdrometer. It has been simulated on Cadence software for finding the values of various components. See Figure 3.12.

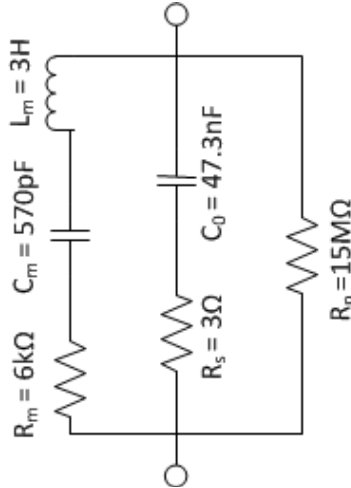


Figure 3.12 Equivalent model of disdrometer with components values

The values for various components are found based on the approach suggested in [32, 33]. Figure 3.13 compares the phase of the frequency response of the simulated model with the phase response of the disdrometer. It is observed that the simulation results provide a good fit to the experimental data.

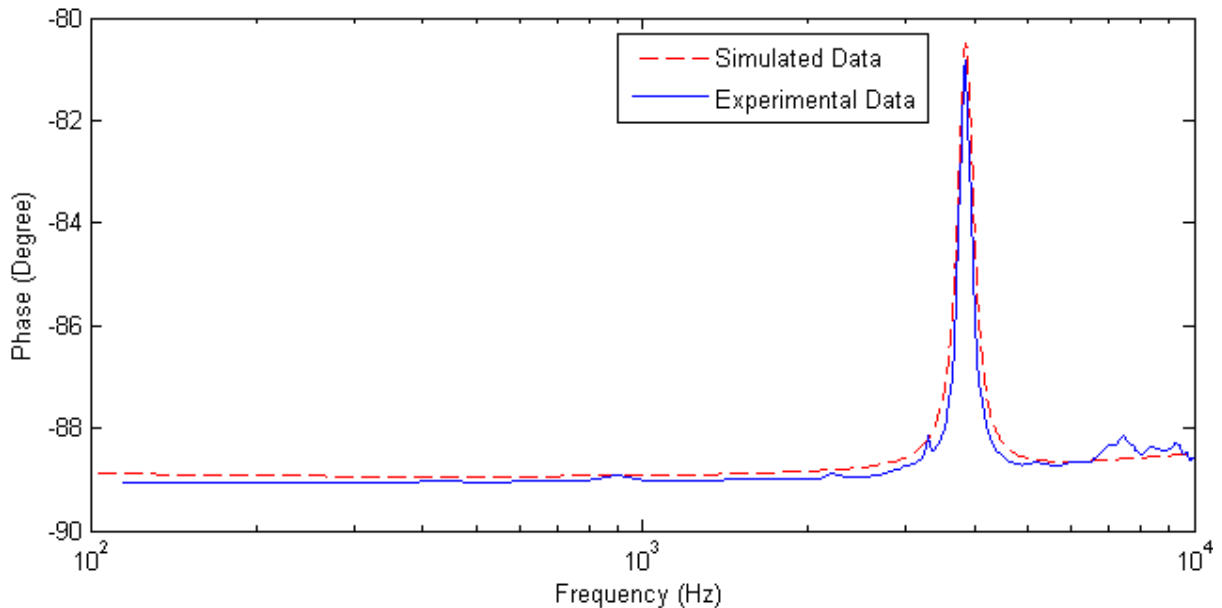


Figure 3.13 Simulated result of the equivalent model of disdrometer

A good agreement between the simulated and the experimental phase indicates that the selected circuit model and the values of different components are representative of the given DWM disdrometer.

3.3 Signal Generation

As was described in the Section 2.2, a piezoelectric material generates electrical charge in response to an external mechanical stress. The PED used for the given application employs the same principle for transduction. The magnitude of the charge generated across the PED because of the raindrop impact can be measured as the voltage U_o . The output voltage of PED, which is proportional to the applied force F_s , is given by:

$$U_o = \frac{d_{33}}{C_o} F_s \quad (3.10)$$

where d_{33} is the piezoelectric constant of the PED and C_o is the capacitance of the sensor.

When a raindrop impinges on the surface of the disdrometer, a complex mechanical interaction occurs between the raindrop and the disdrometer surface. During this interaction, the force F_s and output voltage U_o change rapidly as a function of time [34]. Since the force depends on the raindrop size and its impinging velocity, the output voltage of the disdrometer also depends on these two factors. It was suggested in [34] that the total force accounting for the entire impingement process is a time integral of the voltage mentioned in the eq.(3.10):

$$\int U_o dt = \frac{d_{33}}{C_o} \int F_s dt = \frac{d_{33}}{C_o} M_o = \frac{d_{33} m_o v_o}{C_o} \quad (3.11)$$

where M_o is the vertical momentum of the raindrop impacting the piezoelectric sensor, m_o is the mass of the raindrop, and v_o is the impact (terminal) velocity of the raindrop.

In [35], it was demonstrated that the transfer of the momentum of the raindrop occurs during the impact duration, Δt . The process can be understood with the help of Figure 3.14.

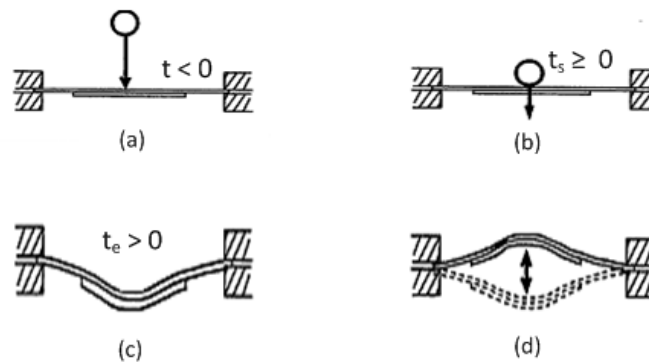


Figure 3.14 Transfer of momentum: (a) raindrop starts falling at $t < 0$, (b) raindrop touches the sensor's surface at $t_s \geq 0$, (c) raindrop get spread in time $t_e > 0$, (d) surface starts oscillating [36]

The raindrop starts falling at time $t < 0$ and hits the disdrometer surface at time $t = t_s (>= 0)$. Subsequently, the raindrop transfers its entire momentum to the PED and spreads over the surface at time $t = t_e$. Beyond $t = t_e$ the PED starts oscillating. The oscillations decay exponentially and finally stop after some time.

The impact duration Δt is given by:

$$\Delta t = t_e - t_s \quad (3.12)$$

Now, the eq. (3.11) can be re-written as

$$\int_{t_s}^{t_e} U_0 dt = \frac{d_{33}}{C_0} \int_{t_s}^{t_e} F_s dt = \frac{d_{33}}{C_0} M_0 = \frac{d_{33} m_0 v_0}{C_0} \quad (3.13)$$

But, the precise determination of the integration boundaries in (3.13) for each drop is technically quite a challenging task [37]. Figure 3.15 shows an example of an output signal U_0 generated by PED when a raindrop hits its surface. As was explained, the output signal starts oscillating beyond the impact end time t_e .

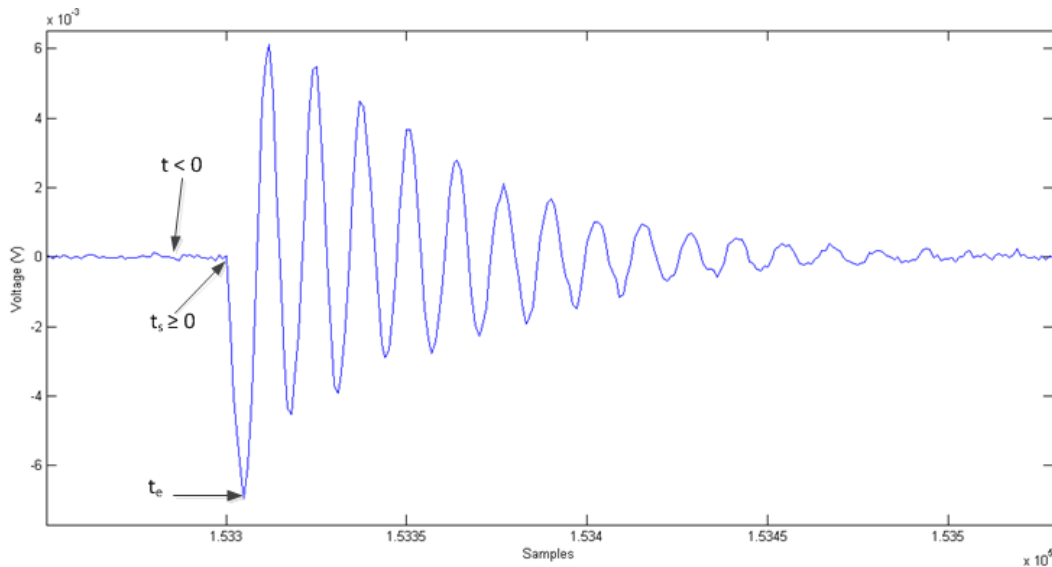


Figure 3.15 Output signal of PED for a raindrop

However, in [38] a similar piezoelectric transducer has been used to measure the kinetic energy of each raindrop. The experimental results presented in [38] suggest that there exists a linear relationship between the first peak of the PED output signal and the raindrop momentum.

In the next section, a measurement setup, using steel balls and DWM disdrometer, has been described which establishes the possibility of using a similar relationship for the DWM disdrometer.

3.3.1 Drop ball Setup

Two test setups using the DWM disdrometer unit and steel ball (bearings) are prepared as shown in Figure 3.16. In both the setups, the steel balls are allowed to fall from a known height with zero initial speed. To a first order approximation, the ball's momentum just before the impact with disdrometer can be calculated from its initial potential energy. When the ball hits the disdrometer surface, it transfers entire momentum to the disdrometer and bends the PED till the time t_e , as shown in Figure 3.14.c. Beyond this bending, the PED starts oscillating and the ball bounces off the disdrometer surface. So, the first peak of the PED's output signal should be proportional to the momentum of the steel ball just before hitting the disdrometer. In the setup, the output of the disdrometer is acquired using National Instrument DAQ USB-6009. The DAQ has a resolution of 14bits and a sampling rate of 48 kS/s.



Figure 3.16 Drop ball setup (a) first design (b) second design

In the first version of the setup, the steel balls were dropped through small steel pipes to fix the point of impact as shown in Figure 3.16.a. But the reproducibility of the results from this setup were not good and a lot of spread in the results was observed. The main reasons for the poor reproducibility were:

1. Mechanical error in constructing the setup.
2. Friction between the balls and the internal surface of the pipe.
3. The rough and non-uniform edges at the openings (both internal and external).

In order to overcome these errors, a second setup was designed as shown in Figure 3.16.b. In this setup, the pipes were removed. Also, the initial height of the balls was reduced in order to keep the point of impact fixed and minimize the effect of air resistance. The reproducibility of this setup was found to be improved. Therefore, we used the second setup for further experiments.

In the experiment, steel balls of various diameters e.g. 1mm, 1.5mm, 2mm, 2.381mm and 2.5mm were used in order to obtain a wide range of momentum. The output of the experiment is shown

in Figure 3.17. In the plot the first peak voltage of each impact is plotted against the momentum of the impact.

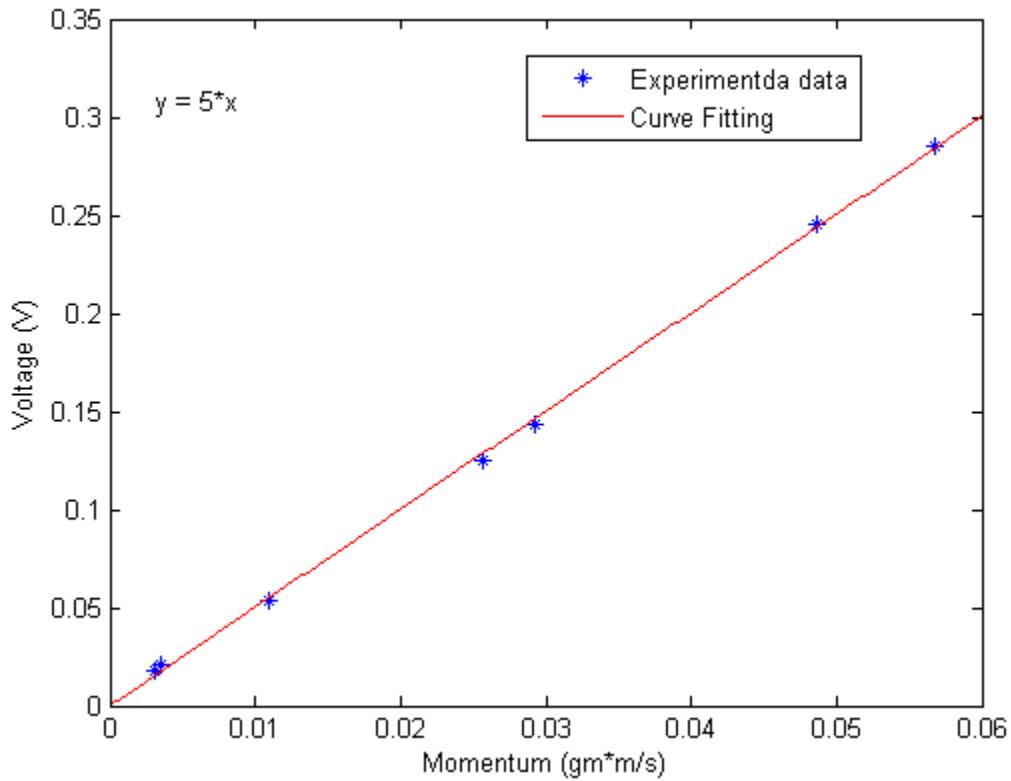


Figure 3.17 Steel ball's momentum vs peak output voltage

In Figure 3.17, it can be observed that for the given inputs there is a first order relation between the first peak voltage and the momentum of the ball. This experiment demonstrates the theory presented in Section 3.3.

Using the results of this experiment as a basis, further experiments were conducted with actual water-drops. The experiments were conducted to derive a relationship between the drop size and the DWM disdrometer output signal.

In the next section, it will be shown that the output of the DWM disdrometer is similar for both the steel ball and water drop impact. Further, using the Drop Tower setup [2] a first order relationship between the momentum of a raindrop and the first peak of the DWM disdrometer's output voltage has been derived.

3.4 Transfer function for the disdrometer

In the previous section, the generation of the DWM disdrometer's output was explained. It was also shown that there exists a relation between the impact momentum and the first peak voltage of the output signal. In this section similar experiments are conducted using a new test setup.

Using this new setup, a relationship between the size of a raindrop and the first peak of the output voltage will be established.

3.4.1 Coherent results

Figure 3.18.(a, b) shows an output signal, both in the time and frequency domains, generated by the drop ball setup, whereas an output signal for a water drop is shown in Figure 3.18.(c, d). A similarity between both the outputs can be observed. Therefore, we infer that the transfer function of the disdrometer for drops should be similar to that of the steel ball setup.

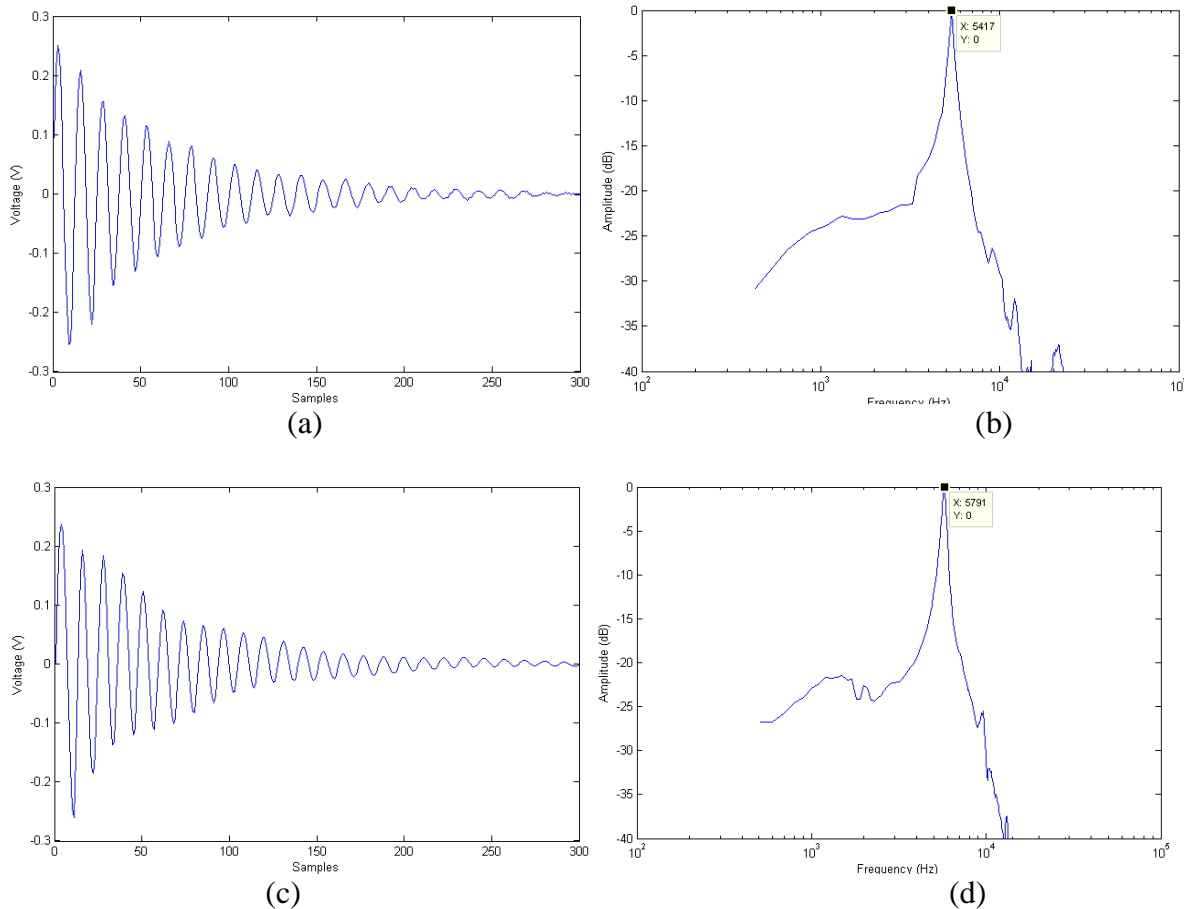


Figure 3.18 Coherence between the output of steel ball impact and raindrop impact (a) disdrometer's output for steel ball impact (b) disdrometer's output spectrum for steel ball impact (c) disdrometer's output for raindrop impact (d) disdrometer's output spectrum for raindrop impact

3.4.2 Drop Tower Setup

Stijn [2] developed an experimental set up called a Drop Tower, which is shown in Figure 3.19. Drops of different diameters are created using a medical syringe and a water reservoir at a height of 14 meters. The size of the drops is measured by weighing them. Also, it is assumed that the drops from the needle are of constant size when the position of the needle is fixed with respect to the water level in the reservoir [2].

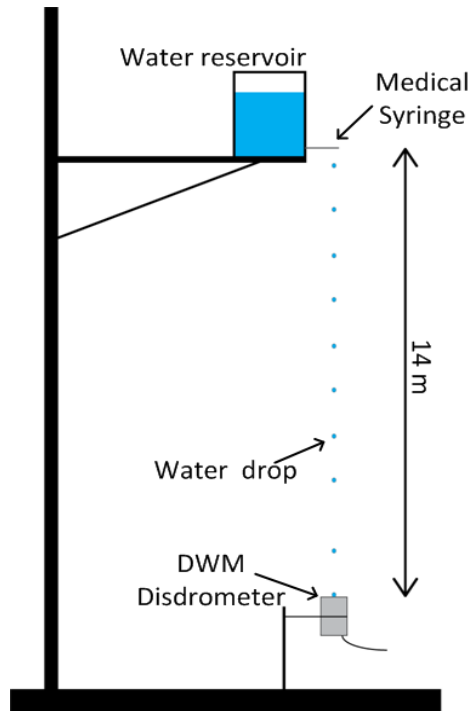


Figure 3.19 Schematic of the drop tower setup in CiTG, TU Delft

Drops of sizes ranging from 2.5mm to 5mm are generated using this setup. Figure 3.20 shows the first peak voltage output of the disdrometer against the momentum of the drops. As expected, a first order relation also exists between the drops' momentum and the first peak of the output signal.

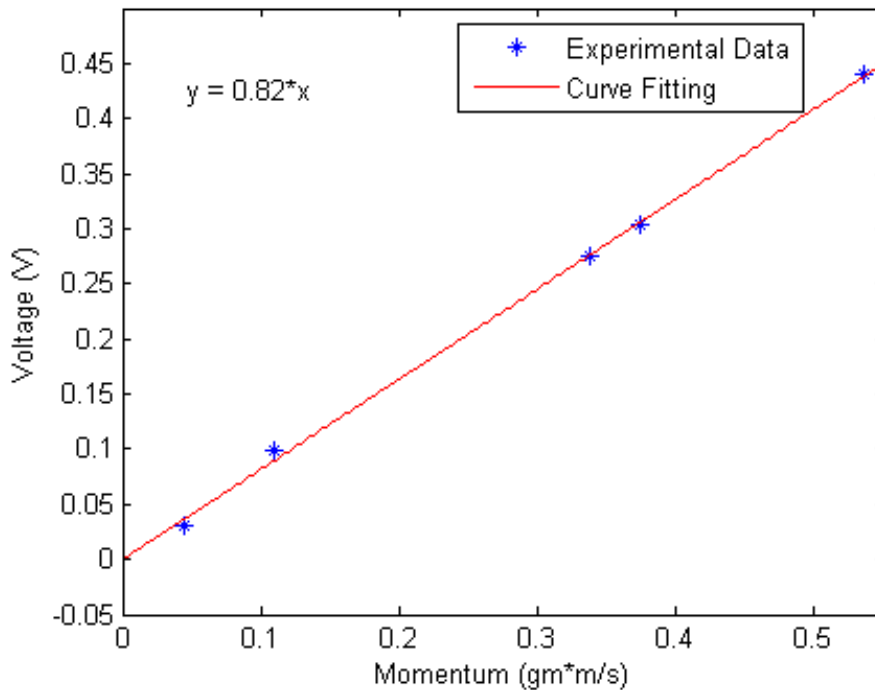


Figure 3.20 Output result of the drop tower experiment

The relation between drop momentum (x) and the first peak of output voltage (y) is given by:

$$V_o = 0.82M \quad (3.14)$$

The above relation holds only for the drops that hit the ceramic part of PED. This relation does not hold if a drop hits the metal part or edge of the PED. In this case, the disdrometer underestimates the size of the drop. This underestimation is known as the edge effect, and will be discussed in the next section.

3.5 Edge Effect

As was mentioned in Section 3.1.2, the DWM disdrometer suffers from an edge effect. This is associated with the boundaries of the disdrometer and has also been observed by [37]. Irrespective of the raindrop distribution over the disdrometer's surface, several drops will hit its edges and produce an inaccurate and underestimated result. When a drop hits the middle of the sensor surface, it transfers all its momentum to the sensor. But, if a raindrop hits the edge, only part of its momentum is transferred. This results in the wrong interpretation of the signal. In other words, a raindrop of 5 mm in diameter can be interpreted as having a 2 mm diameter, if it hits an edge. Schematically, Figure 3.21 illustrates the edge effect.

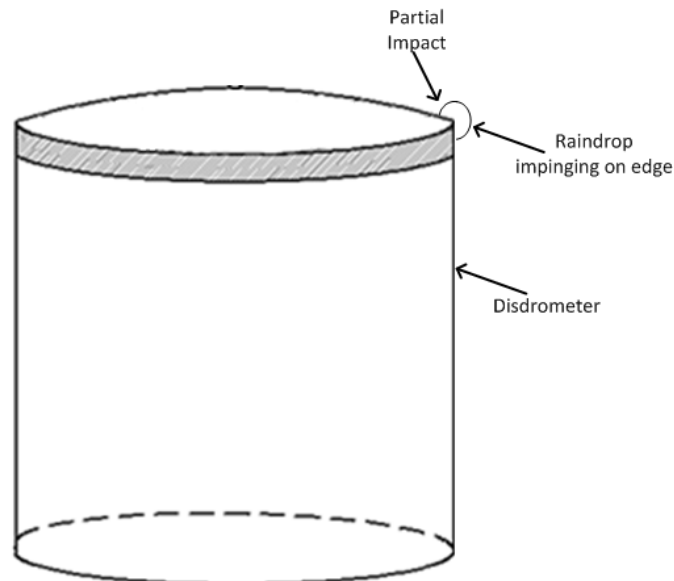


Figure 3.21 Schematic representation of edge effect

One of the commonly used ways to reduce this effect is to use a sensor with larger surface area [13]. In this case, the fraction of raindrops hitting the edge is lower, thus, the edge effect is reduced. But, larger surface area increases the probability of a simultaneous raindrop impact. In the following section, a new method is proposed which can decimate the edge effect using post processing of the acquired data.

3.5.1 Solution to edge effect

During the drop ball experiment, explained in Section 3.3.1, an interesting pattern in the output of the disdrometer was observed. When a ball hits the center of the disdrometer, the transducer generates a sinusoid with a smooth (roughly exponentially) decreasing envelope, see Figure 3.22.a. On the contrary, if the impact is at the edge, the output waveform of the disdrometer is highly distorted. Figure 3.22.b shows the output of disdrometer for a ball hitting on the edge. It can be seen that the envelope for this signal cannot be defined. The same phenomenon was also observed with drops. After repeated experiments, it was concluded that this phenomenon can be used to remove the edge effect, which is one of the major problems with the DWM disdrometer.

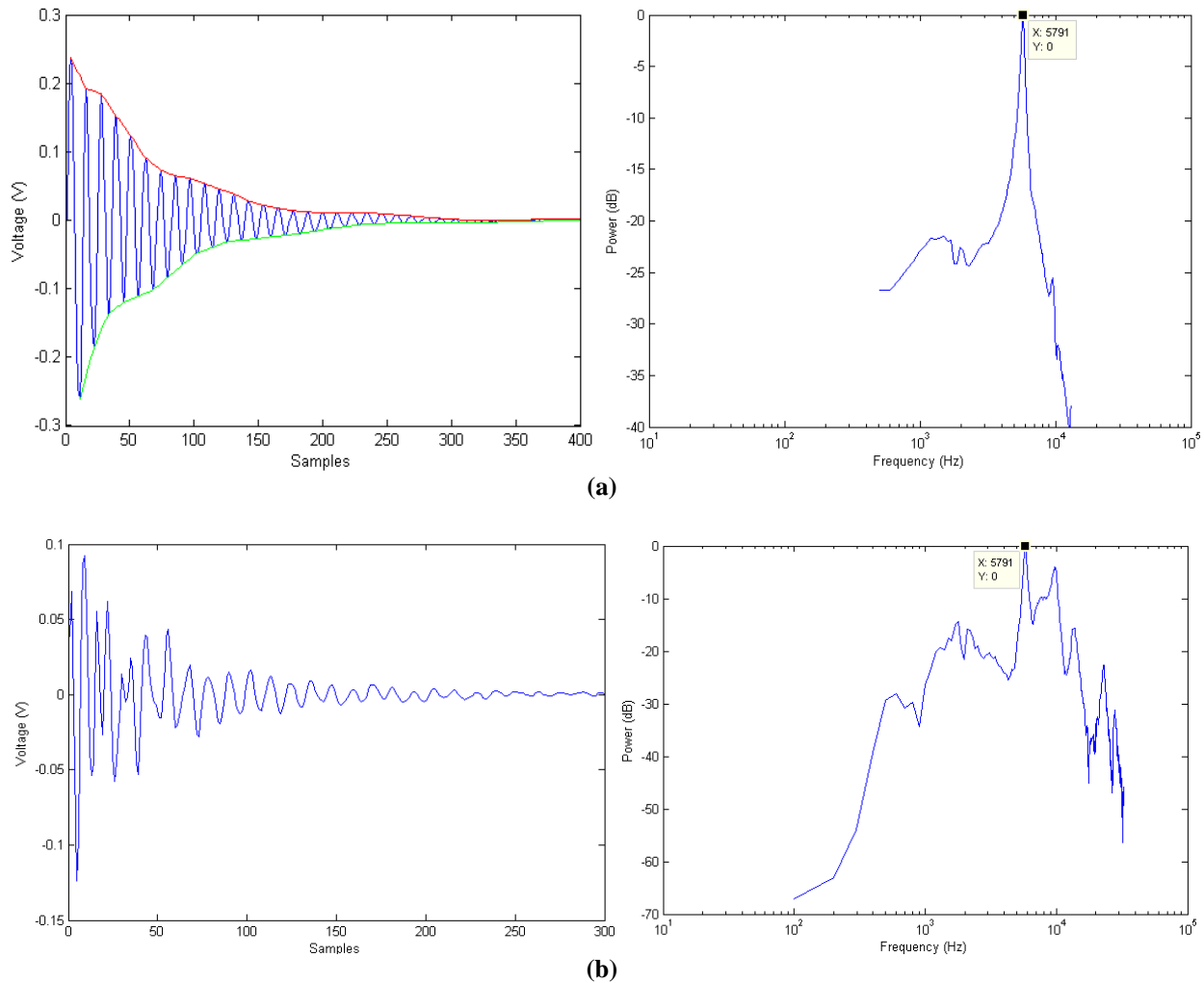


Figure 3.22 Disdrometer output signal of drop impact (a) away from the edge, (b) on the edge

Figure 3.22.a shows the disdrometer output for a drop impinging on the ceramic part of the PED. It can be seen that the power spectrum of the signal has only one tone corresponding to the resonance frequency of the DWM disdrometer. But, several tones are present in the power spectrum for the drop impinging on the edge. This phenomenon can be explained by analyzing the transfer of momentum between the drop and the disdrometer. As shown in Figure 3.23.a,

when a “good” drop impinges at the center of the disdrometer’s hat, all the momentum of the drop gets transferred in the vertical direction. Whereas, when a drop impinges on the edge the momentum gets transferred in all directions, as shown in Figure 3.23.b. This excites all the vibration modes of the PED, generating a highly distorted output signal.

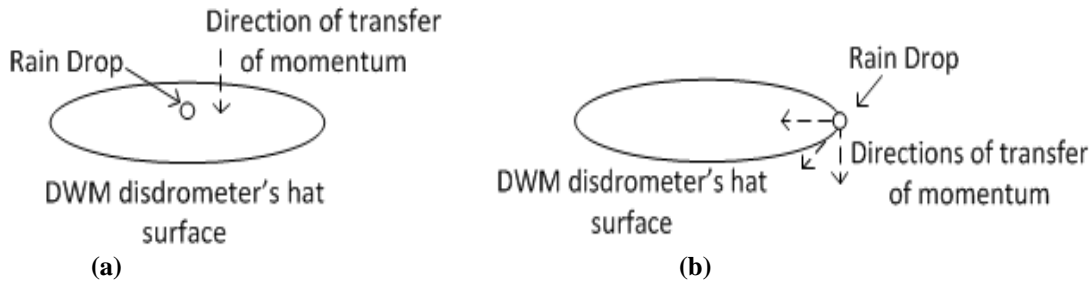


Figure 3.23 Transfer of momentum between a raindrop and DWM Disdrometer (a) drop impinges at the center, (b) drop impinges on the edge

Based on this observation, an algorithm given in Appendix B has been developed to detect the edge impact on the DWM disdrometer. It is based on the observation that for a “good” drop, the difference between the upper envelope and the lower envelope should be monotonically decreasing function. This property, to a first order, can be used to distinguish between good drops and edge drops. But, practically there will be some discontinuity even for the good drops. So, the algorithm should be efficient to tolerate some errors.

The algorithm was applied to 14,262 drops which comprised both edge and center impact drops. From this set 13,618 drops were correctly categorized into edge or centre drops. Only 644 drops (4.51% of total set) were not categorized correctly.

3.5.2 Depth of the Edge Effect

More experiments were conducted to understand the depth to which the edge effect can be observed from the disdrometer boundary. In this experiment, the diameter of the disdrometer ($D = 50\text{mm}$) was divided into 10 equidistant points and the results of drop impacts on each point were measured as shown in Figure 3.24.



Figure 3.24 DWM disdrometer to test the depth of edge effect

It was observed that the edge effect mainly occurs when the impact on the edge of the ceramic or on the metal part of the PED. As the impact points move towards the ceramic or towards the center of the PED, the edge effect fades away. Pictographically the region of the edge effect can be seen in Figure 3.25.

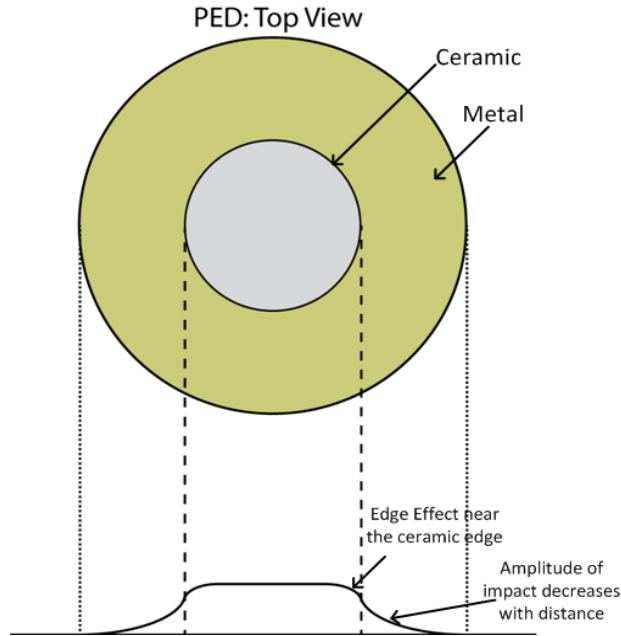


Figure 3.25 Schematic representation of the extent edge effect on PED

3.6 Summary

In this chapter, various aspects of the DWM disdrometer have been described. In the first section the design of two important parts of the DWM disdrometer i.e. the PED and the hat of the sensor were discussed. A guideline for selecting the disdrometer's transducer from commercially available PED was derived. In the next section, based on the impedance response of the disdrometer, an equivalent electrical circuit model was proposed and verified. This was followed by an explanation of the signal generation process in the DWM disdrometer, which gave a direction for a possible relation between the first peak voltage of the output signal to the momentum of a raindrop. To investigate this, a drop ball setup was designed and a relationship was derived between the momentum and the output signal. Observing the coherence between signal output of disdrometer for a steel ball impact and for a raindrop impact, experiments were done for water drop using drop tower setup. In this experiment a first order relation between the momentum of raindrop and the output voltage was derived. In the last section of the chapter an important error source for the DWM disdrometer, i.e. the Edge effect, was discussed for which an innovative solution has been proposed and successfully verified. In the next chapter, a readout circuit, using discrete components, for the DWM disdrometer will be designed.

Chapter 4 Circuit Design and Measurements

This chapter discusses the design of the readout circuit board for the (Department of Water Management) DWM disdrometer. The design specifications for the circuit are derived in Section 4.1. The measurement setup for testing the system is discussed in Section 4.2. Based on the specifications and the measurement setup, a system-architecture for the readout circuit is proposed in Section 4.3. The motivation behind the choice of various circuit components is given in Section 4.4. The designed PCB and its schematic presented in Section 4.5. The measurements results are presented in Section 4.6.

4.1 Specifications

Being a novel idea, very few electrical specifications of the DWM disdrometer were available. Also, as described in Chapter 3, the piezoelectric diaphragm (PED) and the design of the DWM disdrometer's packaging are still an active area of research. This makes the design of the readout circuit more challenging.

In the current section, a list of specifications has been derived based on the existing literature, known environmental conditions and the experiments presented in Chapter 3. The list includes:

1. Dynamic Range
2. Bandwidth
3. Noise
4. Power

The specifications are chosen in a way to enhance the tolerance of the overall system to future changes in the disdrometer's design.

4.1.1 Dynamic Range

The Dynamic Range (DR) of a circuit is defined as the ratio between the largest and the smallest voltage of input signal which can be measured. For the readout circuit of the DWM disdrometer, the DR is equal to the output range of the PED transducer. Most of the available disdrometer's claim to measure raindrops with sizes ranging from 0.5mm to 5.5mm in diameter. We aim to measure the raindrops with diameter ranging from 0.3mm to 6mm as an improvement over existing designs. Therefore,

$$DR \geq 20 \cdot \log \left(\frac{\text{output voltage for 6mm raindrop}}{\text{output voltage for 0.3mm raindrop}} \right) \quad (4.1)$$

Using the empirically derived transfer function (eq.(3.14)) described in Section 3.4.2 the DR for the circuit should be greater than 98dB to cover the specified range of raindrop's diameter, The detailed computation is presented in Appendix C.

4.1.2 Bandwidth

The bandwidth requirement of the readout circuit for the DWM disdrometer depends on the resonance frequency of the disdrometer. Most of the commercially available low cost PED have resonance frequencies in the range of 500 – 5k Hz. As was described in Section 3.2.2, the resonance frequency of the disdrometer depends on its packaging. Since the packaging of the disdrometer is still evolving, the designed circuit should have a wider bandwidth to accommodate variation in the resonance frequency. It has been observed that the resonance frequency of the system can shift up to 4 kHz due to packaging. Therefore, a bandwidth of 10 kHz was chosen for the readout circuit.

4.1.3 Noise

As was explained in Section 4.1.1, the minimum raindrop which needs to be measured is 0.3mm along the diameter. Since the noise specification of the circuit depends on the smallest raindrop, the output voltage of the DWM disdrometer needs to be measured for the 0.3mm (along the diameter) drop. The derivation of the output voltage is given further:

Using the eq (2.1) and eq (2.3) the terminal velocity, ' v_t ' and the mass, ' m_0 ' of the 0.3mm (along the diameter) drop can be computed as:

$$m_0 = 14\mu\text{gm}, v_t = 1.73\text{m/s}$$

Furthermore, using eq.(3.14), the expected output voltage of DWM disdrometer can be calculated as:

$$V_0 = 0.82 * M_0 = 0.82 * m_0 * v_t = 19.4\mu\text{V} = 13.8 \mu\text{V}_{\text{rms}}$$

A margin of 6dB has been chosen in order to reliably measure this output. Therefore, the system should have the total input referred noise less than $7\mu\text{V}_{\text{rms}}$.

4.1.4 Power

As was discussed in the Chapter 1, the DWM disdrometer is to be used as a part of a wireless weather station powered by solar panel. Therefore, the power specification for the readout circuit has to be derived from the power budget analysis of the complete weather stations. This analysis is explained in Appendix C in detail. The power specification for the readout circuit is derived as 20mA@5V.

4.1.5 Specifications Summary

Table 4-1 summarizes the derived specifications:

Table 4-1 System specification

Parameter	Specification
Dynamic Range	98dB
Bandwidth	10kHz
Noise	$7\mu V_{\text{rms}}$
Power	20mA@5V

4.2 Measurement Setup

Figure 4.1 shows the schematic of the measurement setup used for testing the designed readout circuit with the DWM disdrometer.

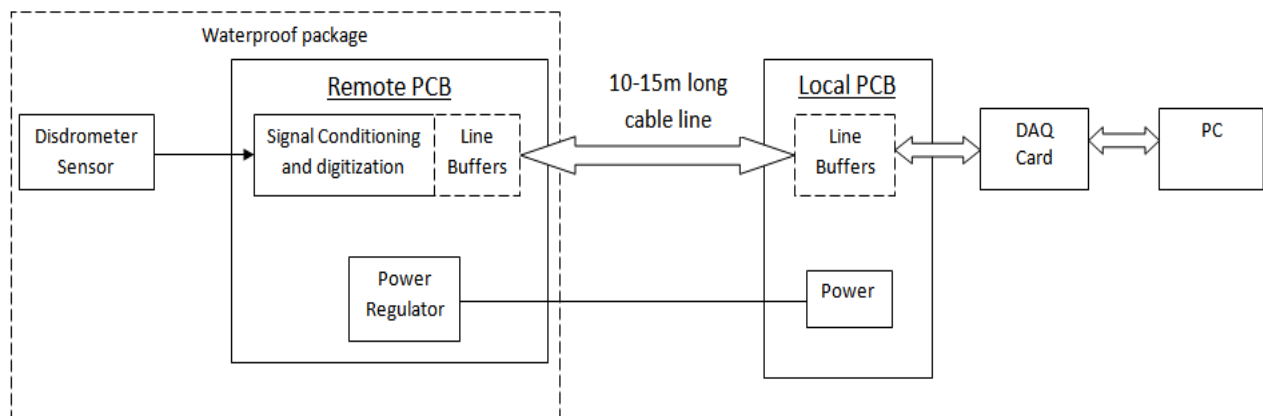


Figure 4.1 Measurement setup

Since, water drops will be used during the testing; the measurement setup has been divided into two parts i.e.

1. Remote Setup: The DWM disdrometer and the readout circuit will be on the remote side of the setup. The readout circuit board will be encapsulated inside the disdrometer package as shown in Figure 4.2.



Figure 4.2 The remote part of the measurement setup

2. Local Setup: The processing required during the measurements will be done at the local end of the setup. A Labview code has been developed to collect the data bits from the ADC using NI USB-6363 DAQ.

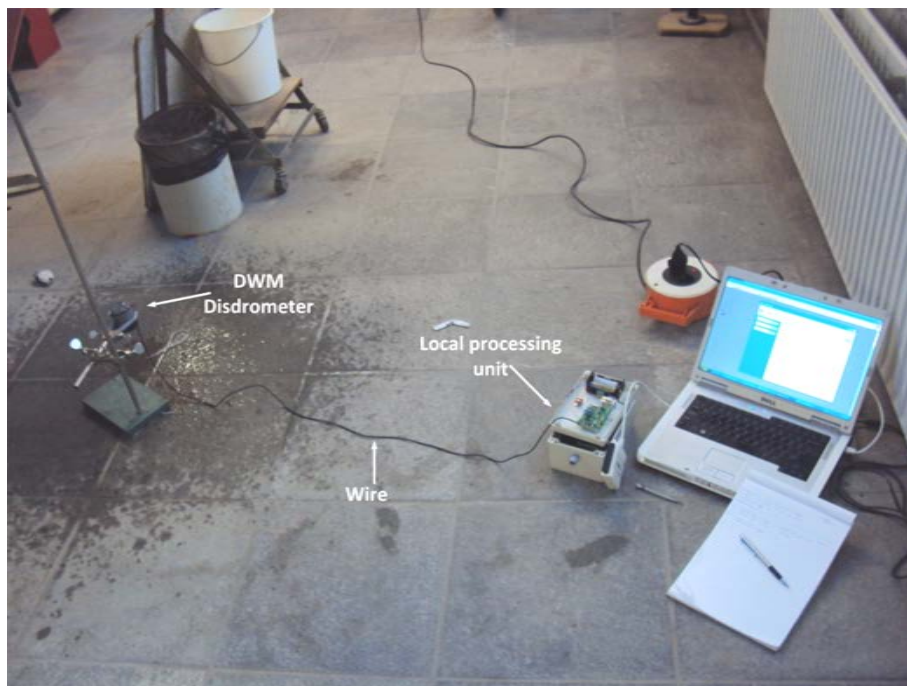


Figure 4.3 Measurement setup

Figure 4.3 shows the actual measurement setup. For the mentioned setup and specifications a readout circuit has been designed and presented in the next section.

4.3 System Architecture

Figure 4.4 shows the typical architecture of a sensor readout circuit. In this architecture, the output of the transducer is amplified by the amplifier 'Amp'. The 'ADC' digitizes the amplified signal and provides a digital output to a microcontroller or other processing unit.

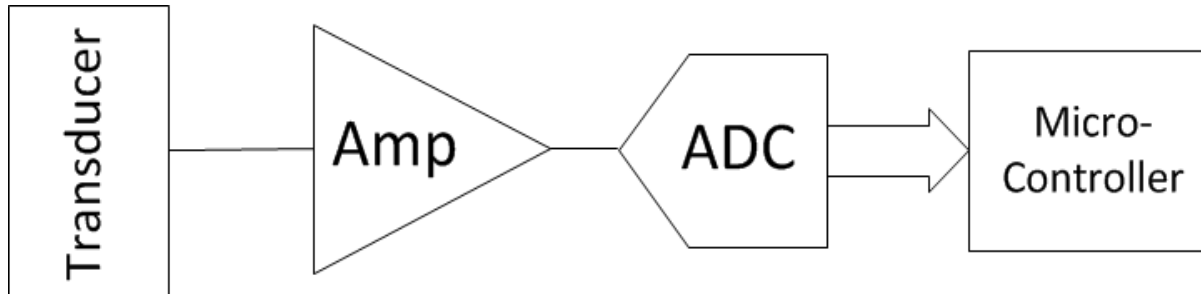


Figure 4.4 Typical sensor readout system

4.3.1 Amplifier

There are various topologies for the amplifier depending on the electrical characteristics of the sensor. In the Section 3.2, it was explained that the transducer of the given DWM disdrometer is effectively a capacitive sensor. Two popular topologies are often used for a capacitive sensor [39], namely:

1. Charge mode amplifier
2. Voltage mode amplifier

Charge Mode Amplifier

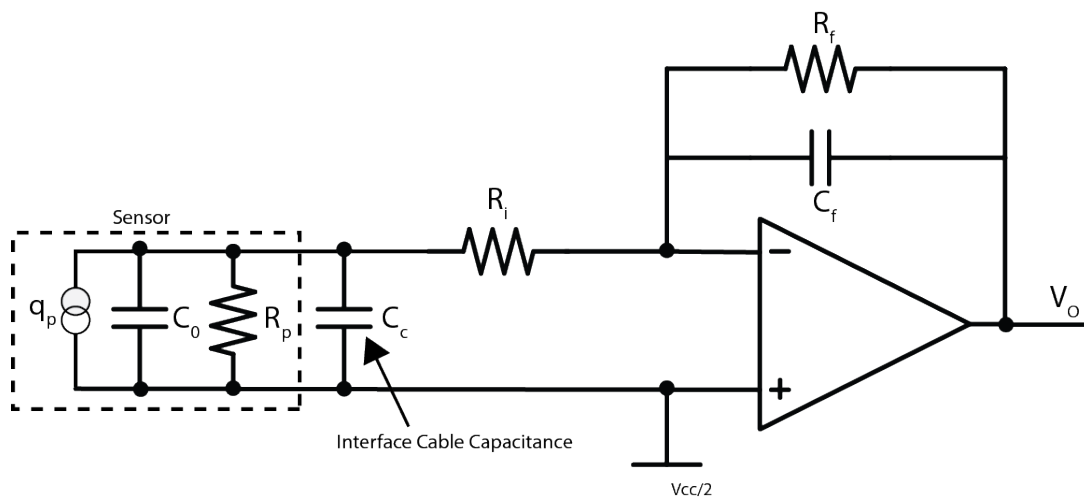


Figure 4.5 Charge mode amplifier circuit

Figure 4.5 shows the circuit for a charge mode amplifier. As discussed in Section 3.2, the capacitor ' C_0 ' and the parallel resistor ' R_p ' represent the simplified electrical model of the DWM disdrometer. ' q_p ' is the charge generated by the piezoelectric material. The capacitor ' C_c ' is the stray capacitance associated with the interface cable.

In this configuration, the amplifier generates an output voltage by balancing the charge produced by the transducer. It balances the charge by charging the feedback capacitor ' C_f '. The feedback resistor ' R_f ' provides a dc bias path for the negative input of the amplifier. It also prevents the amplifier from drifting into saturation. Assuming, $R_i \ll R_p$, the output voltage of the charge amplifier is given by:

$$V_o = -q_p \left(\frac{sR_f}{1 + sR_f C_f} \right) \left(\frac{1}{1 + sR_i (C_o + C_c)} \right) + \frac{V_{cc}}{2} \quad (4.2)$$

Where V_o is the amplifier output and q_p is the charge produced by the transducer.

The frequency response of the circuit is:

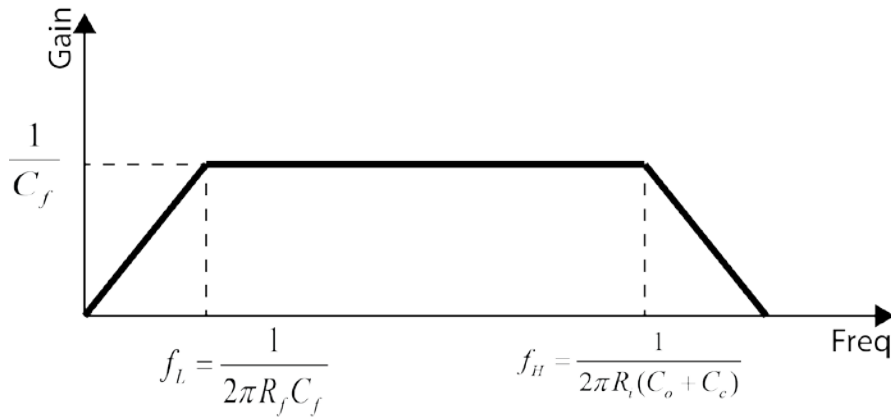


Figure 4.6 Frequency response of charge mode amplifier

Figure 4.6 shows the frequency response of the circuit. The upper cut off frequency of the circuit is defined by resistor ' R_i ', and the parallel combination of PED's capacitor ' C_o ' and the stray capacitance ' C_c '. As was mentioned in Section 3.1, the design of DWM disdrometer is not yet fixed. Therefore, a variation in the value of the PED's capacitor ' C_o ' changes the bandwidth of the circuit.

1. An increase in $C_o + C_c$ reduces the bandwidth of the circuit, which affects the signal response of the circuit.
2. A decrease in $C_o + C_c$ increases the bandwidth of the circuit, which affects the noise performance of the circuit.

This uncertainty in the circuit bandwidth makes the charge mode architecture less attractive or the DWM disdrometer.

Voltage Mode Amplifier

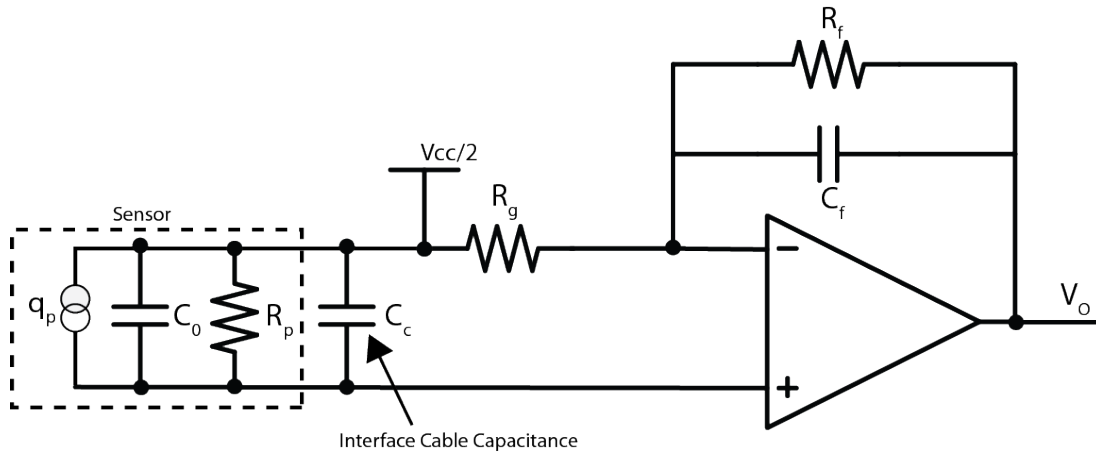


Figure 4.7 Voltage mode amplifier circuit

The voltage mode amplifier for a capacitive sensor is shown in Figure 4.7. Because of its high input impedance, this configuration is frequently used for various applications making use of piezoelectric transducers [40, 41]. The output voltage of the voltage amplifier circuit is given by:

$$V_o = q_p \left(1 + \frac{R_f}{R_g} \left[\frac{1}{1 + sC_f R_f} \right] \right) \left(\frac{sR_p}{1 + sR_p (C_0 \parallel C_c)} \right) + \frac{V_{cc}}{2} \quad (4.3)$$

Where V_o is the amplifier output and q_p is the charge produced by the transducer.

The frequency response of the circuit is: $\left(1 + \frac{R_f}{R_g} \right) \left(\frac{1}{C_0 + C_c} \right)$

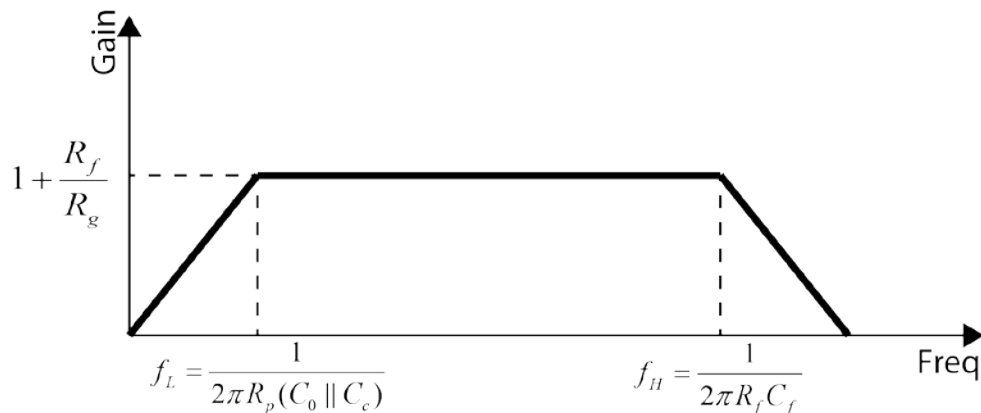


Figure 4.8 Frequency response of the voltage mode amplifier

Figure 4.8 shows the frequency response of the voltage mode circuit. Unlike the charge mode amplifier, the upper cutoff frequency is independent of the PED properties and can be set

independently. As shown, the properties of the PED affect the lower cutoff frequency of the circuit which is not a concern for the disdrometer application. So, a voltage mode of amplifier is used for the DWM disdrometer's readout circuit.

4.3.2 Analog-to-Digital Converter (ADC)

The ADC is chosen based on the required DR, noise (both thermal and quantization noise), power consumption and its sampling speed. As was mentioned in the Section 4.1, the system should have a DR of at least 98dB. This translates into a minimum of 17 bit resolution for the ADC. Also, the specified bandwidth of the signal is 10 kHz. Therefore, the sampling speed of ADC should be 20kSPS at least.

Usually, an ADC consumes most of the available power in similar readout circuits. Under the assumption that the amplifier and power regulator consumes 5mA@5V, the rest of the power can be allocated to ADC. Therefore the power consumption of the ADC should be less than 15mA@5V. In the Section 4.4.2, the ADC selected for the given purpose is presented.

4.3.3 Proposed Circuit Design

Figure 4.9 shows the schematic of the proposed circuit. The capacitor ' C_{hf} ' and the resistor ' R_g ' acts as a high pass filter and help in reducing the DC power consumption of the circuit. Furthermore, a low pass filter is implemented using capacitor ' C_{lf} ' and the resistor ' R_{lf} '. It is added to keep the circuit flexible and robust to noise. A simplified schematic of the proposed design is presented in Figure 4-11.

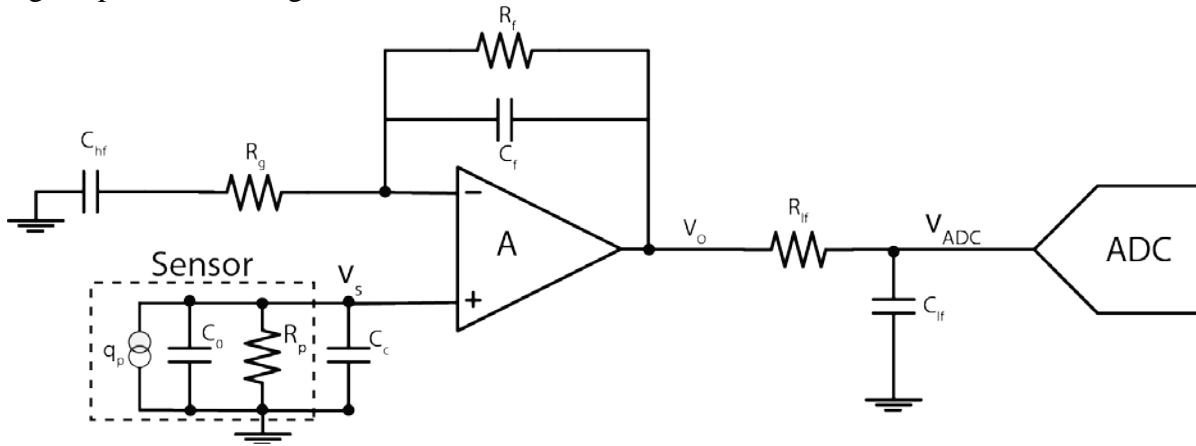


Figure 4.9 A simplified schematic of the proposed circuit

If ' V_s ' is the output signal of the sensor, then the amplifier output, assuming proper biasing of the Op-Amps, is given by:

$$V_o = q_p \left(\frac{sR_p}{1 + sR_p(C_0 \parallel C_c)} \right) \left(1 + \frac{R_f}{1 + sC_f R_f} \frac{sC_{hf}}{1 + sR_g C_{hf}} \right) \quad (4.4)$$

Figure 4.10 shows the frequency response of the proposed circuit:

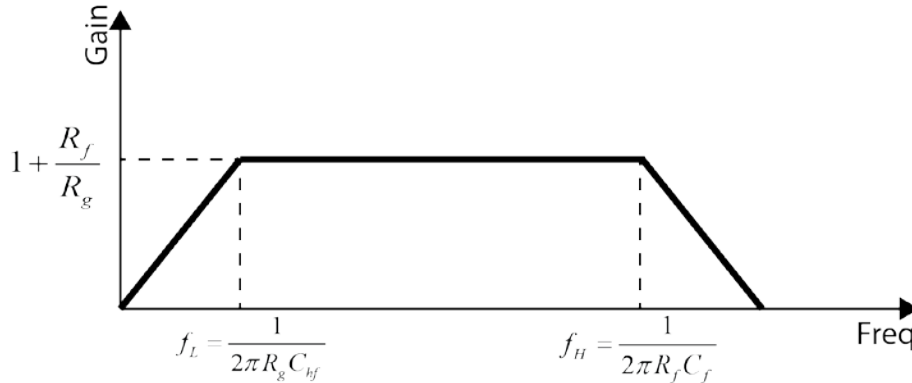


Figure 4.10 Frequency response of the proposed circuit at amplifier output

4.4 Component Selection

The circuit proposed in the Figure 4.9 is implemented with the specification given in the Table 4.1. A careful selection of the components is made in order to achieve the required system performance. The following section presents the motivation for selection of the specific components for the circuit.

4.4.1 Amplifier – LMV851 [42]

As was mentioned in Section 4.1, the readout circuit has to be low noise and low power for the required bandwidth. LMV851, by Texas Instruments, offers the most suitable specifications among the available amplifiers. It is a CMOS input, low-power op amp IC. Its specifications are following:

1. Input referred noise voltage density = 11 nV/ $\sqrt{\text{Hz}}$
2. Input bias current = 1 pA
3. Current consumption = 0.4 mA @3.3V
4. GBW = 8 MHz
5. 1/f noise = 10nV/ $\sqrt{\text{Hz}}$ @ 1 kHz

Since, the resonance frequency of the DWM disdrometer is always higher than 2 kHz, the flicker noise of the amplifier has been digitally filtered out, thus, need not to be consider.

4.4.2 Analog-to-Digital Converter (ADC) – AD7767-2 [43]

For the proposed circuit, a low-power and low-noise ADC with a minimum of 17 bit resolution and 20 kSPS is required. But it should be re-stated that the specification for the required resolution of ADC is based on the empirically obtained transfer function given by eq. 3.12. Water drops of size ranging from 2mm to 5mm have been used to derive this transfer function. It has been assumed, the given transfer function also hold for very small drops. But this may not be true because of the complex interaction between the drop and the impinging surface. Therefore, to manage this uncertainty, an ADC of higher resolution needs to be selected.

For the given specifications and uncertainty the AD7767-2, from Analog Devices, suits best to these requirements. It is a high performance, 24-bit, oversampled SAR ADC. Its specifications are as follow:

1. A large dynamic range of 114.5 dB.
2. A Sampling rate of 32 kSPS.
3. Exceptionally low power ADC: 8.5 mW@ 2.5 V
4. Low thermal noise floor: -140 dB.

The AD7767-2 includes an on-board digital filter that eliminates out-of-band noise by filtering the oversampled input voltage. Therefore, AD7767-2 is a good choice for a low-noise and low-power DWM Disdrometer.

4.4.3 Voltage Reference (V_{ref})-MAX6126 [44]

The precision and stability of the voltage reference directly affects the overall system accuracy. If the reference voltage is unstable, the 24-bit ADC would not be as much effective. Therefore, an ultra-high-precision, ultra-low-noise, and series voltage reference MAX6126 is used for the proposed circuit.

By making use of the precision thin-film resistors and laser trimming techniques, MAX6126 provides an initial accuracy of 0.02% (max) and a temperature coefficient of 3ppm/ $^{\circ}$ C. It has a low flicker noise of $1.3\mu V_{p-p}$ and wideband noise of $60nV/\sqrt{Hz}$. In order to obtain an improved wideband noise of $35nV/\sqrt{Hz}$, a $0.1\mu F$ capacitor is added at the noise reduction pin.

4.4.4 Passive components

The values of the passive components in the circuit depend on the gain and the bandwidth specifications of the circuit. The values of the resistors are obtained from the gain specifications:

$$Gain = \left(1 + \frac{R_f}{R_g} \right) \quad (4.5)$$

If a gain of 2 is required, then:

$$R_f = R_g$$

Before selecting the actual value of the resistors, their noise contribution and the stability of the amplifier needs to be consider. After selecting the resistor, the values of the capacitors can be obtained from the specified upper and lower cutoff frequency for the circuit.

4.5 PCB Design

Figure 4.11 shows the complete schematic of the readout circuit. An important specification for designing the PCB is its size. As was explained in Section 4.2, the PCB is to be encapsulated in

Figure 4.12 shows the placement of the components on the designed PCB. The components are placed only on top side of the PCB. Since this is a mixed signal PCB, it is virtually divided into two sections: analog and digital, with ADC as the bridge. All the analog signal tracks and the components are placed on one side of the PCB and all the digital tracks and the components on the other. The brown line in the Figure 4.12 shows the internal ground plane. Both the section are separated and joined under the ADC to avoid any digital noise on the analog part of the ground plane.

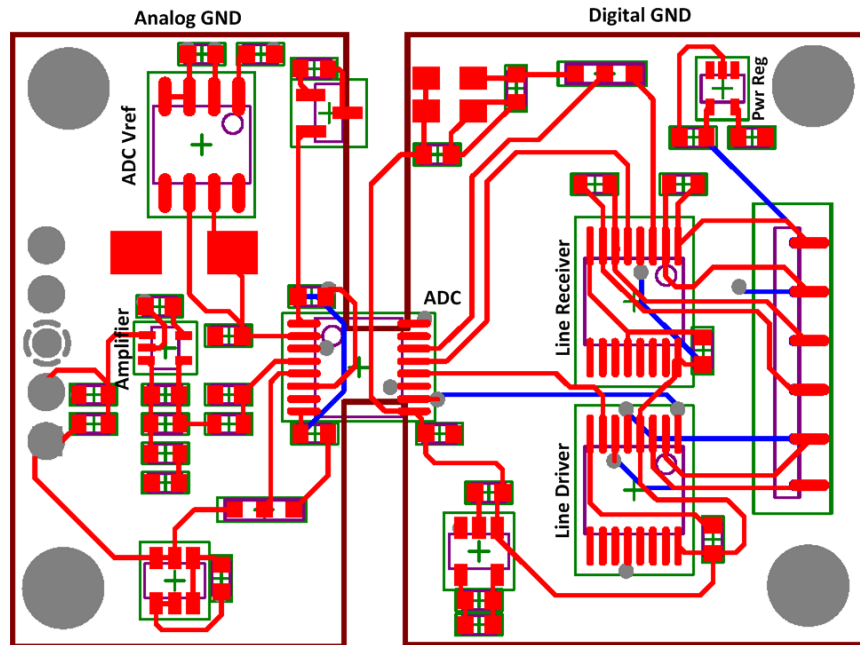


Figure 4.12 Layout of PCB

A four layer PCB of size 32mm x 52mm has been designed. Figure 4.13 shows the designed PCB.

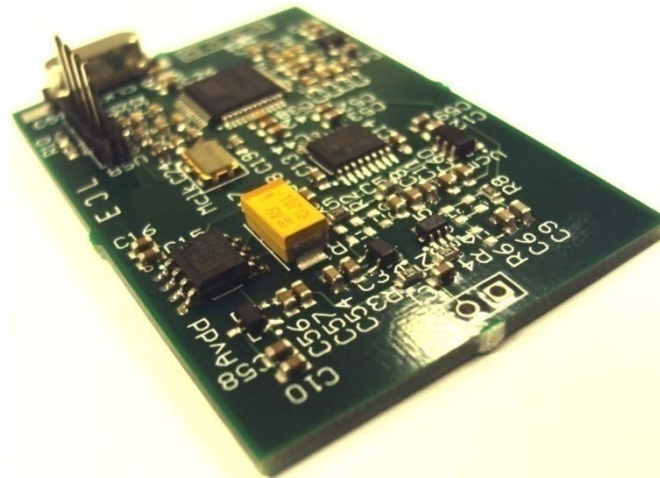


Figure 4.13 Designed PCB for the DWM disdrometer

4.6 Measurements Results

The readout circuit designed in the previous section has been used to conduct various experiments. The current section presents and discussed the obtained measurement results.

4.6.1 Power Consumption

The power consumption of the analog part of the readout circuit is measured to be $17.8\text{mA}@5\text{V}$, which is well below the specifications. Furthermore, the ADCs and its peripheral ICs can be disabled in the standby mode i.e. when there is no rain. This reduces the power consumption of the circuit to $1.3\text{mA}@5\text{V}$.

4.6.2 Noise Measurements of readout circuit

Figure 4.14 shows the input referred noise of the readout circuit. The noise of the readout circuit, without the transducer, after digitization was measured to be $6.05\mu\text{V}_{\text{rms}}$. This is slightly higher than the calculated (refer to Appendix E) input referred noise of $5.67\mu\text{V}_{\text{rms}}$.

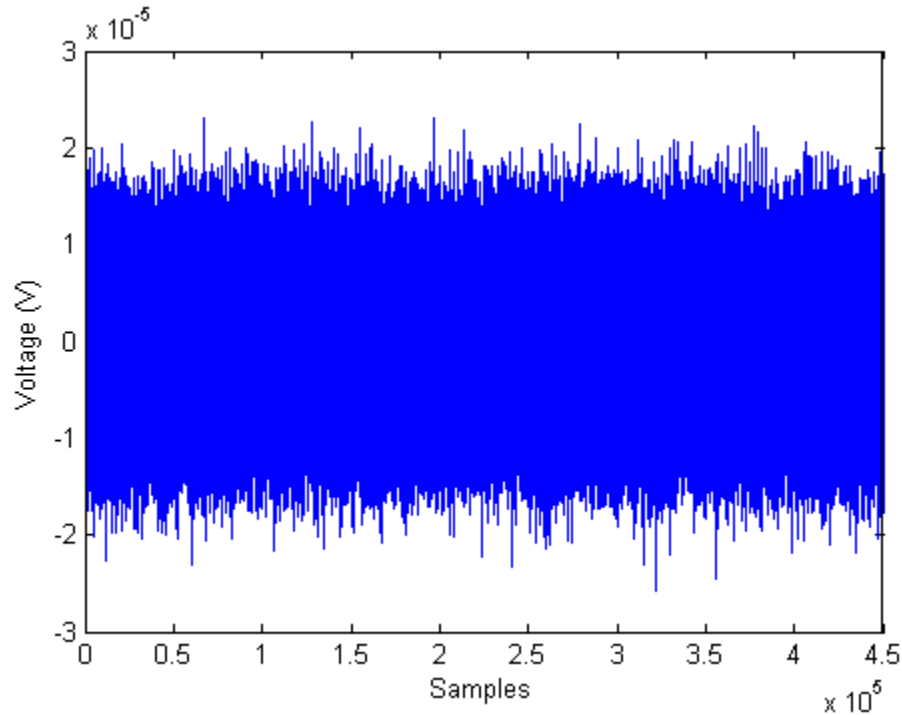


Figure 4.14 Readout circuit noise at ADC's output

4.6.3 System Noise Performance

The noise performance of the complete system, including the noise of the transducer, is shown in Figure 4.15. It shows the output of a disdrometer without any drop impact. This represents the noise of the system and was measured to be $7.8\mu\text{V}_{\text{rms}}$. The increase in the noise compared to previous measurement is because of the noise added by the transducer. In Section 4.1.3, the required noise performance of the system was mentioned to be $7\mu\text{V}_{\text{rms}}$. Therefore, the noise of the complete system is slightly above the given specifications. But a margin of 6dB was kept to

measure the smallest drop of size 0.3mm along diameter. Therefore, this noise performance is still acceptable.

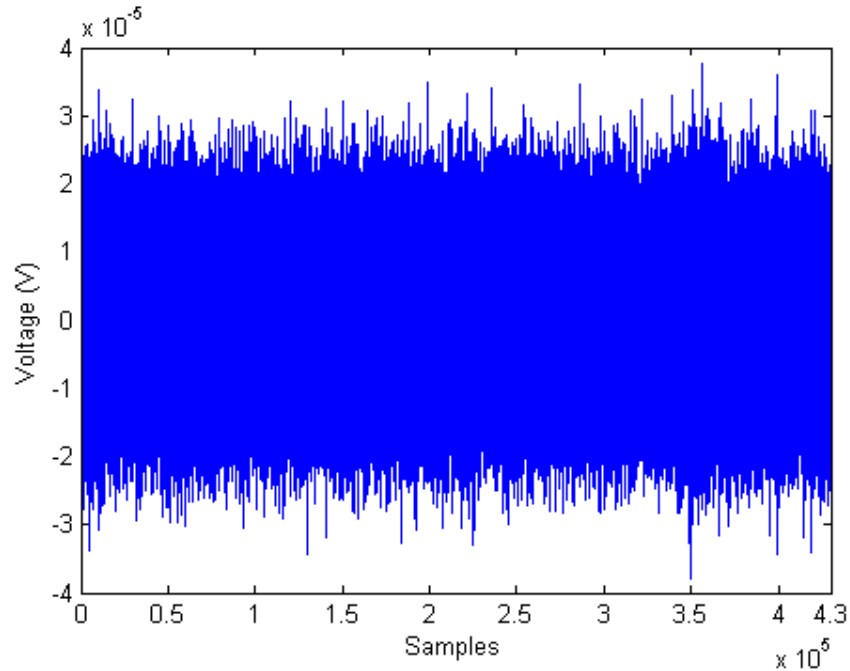


Figure 4.15 Noise performance of the disdrometer

4.6.4 Reproducibility of a fixed impact point

To analyze the reproducibility of a disdrometer, another experiment was done with a modified drop tower setup. In the original drop tower setup, the point of impact of was not controlled and drops were impinging all over the disdrometer surface. In the new setup, the height of the water reservoir is reduced from 14m to 0.5m. Now, the small height of the reservoir ensures a fixed impinging point.

A free fall of 0.5m is not sufficient for drops to reach their terminal velocity. But the actual terminal velocity, and thus momentum, is not required for this experiment. It can be assumed to a first order approximation that all the drops of same size which are falling from a same height, under similar environmental conditions acquire same momentum before impinging on the disdrometer.

Figure 4.16 shows the output of the DWM disdrometer for 8 impacts from the 8 drops of same size.

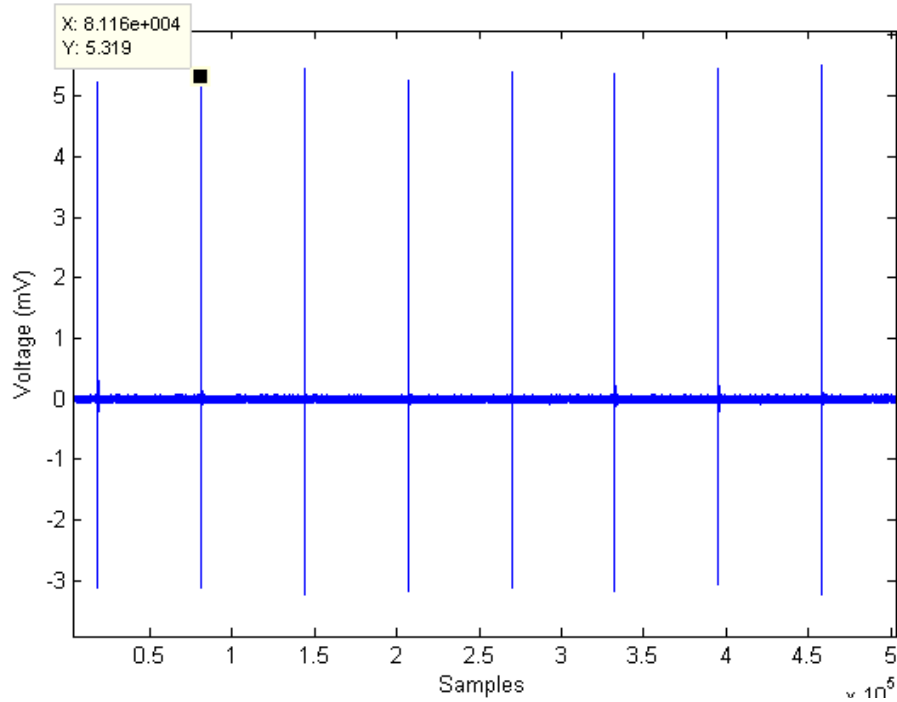


Figure 4.16 Reproducibility of disdrometer's output

Table 4-2 gives the first peak voltage for the 8 impact. The standard deviation in the output was calculated to be $76.7\mu\text{V}$ which is equal to $\pm 1.4\%$ of accuracy. This shows that the output of the complete disdrometer system is reproducible to a very good accuracy.

Table 4-2 Drop peak voltage for reproducibility test

Drop #	First peak voltage (mv)
1	5.3147
2	5.3185
3	5.4579
4	5.2965
5	5.4070
6	5.3757
7	5.4609
8	5.4981
Std Dev	0.0767

4.6.5 Transfer Function

The drop tower measurements conducted in Section 3.4.2 were repeated with the new setup. Figure 4.17 presents the result of the experiment. The x -axis represents the momentum (M) of the drops and y -axis represents the first peak voltage (V_0) of disdrometer output. As is shown in the figure, the relation between the two drop's momentum and first peak voltage is given by:

$$V_0 = 0.83M \quad (4.6)$$

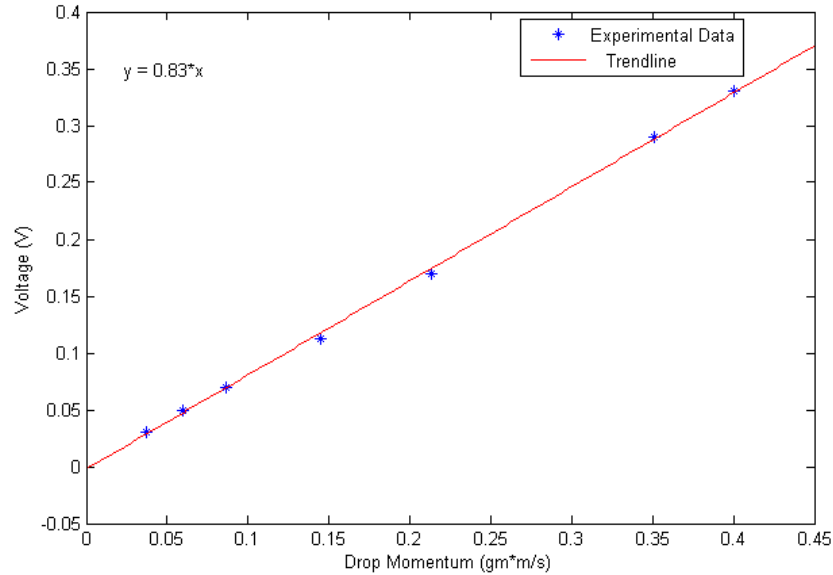


Figure 4.17 Result of drop tower measurements with new setup

This result again confirms the conclusion drawn in Section 3.3, i.e. the voltage of the first peak of disdrometer output is a linear function of the drop's momentum. In other words, the size of a drop can be calculated from the first peak voltage of the disdrometer's output.

4.6.6 Small drop output signal

The good noise performance of the new DWM disdrometer system makes it possible to measure drops of size smaller than 1mm in diameter. Figure 4.18 shows the output of the disdrometer for drops of size ranging from 0.4mm to 0.6mm along the diameter.

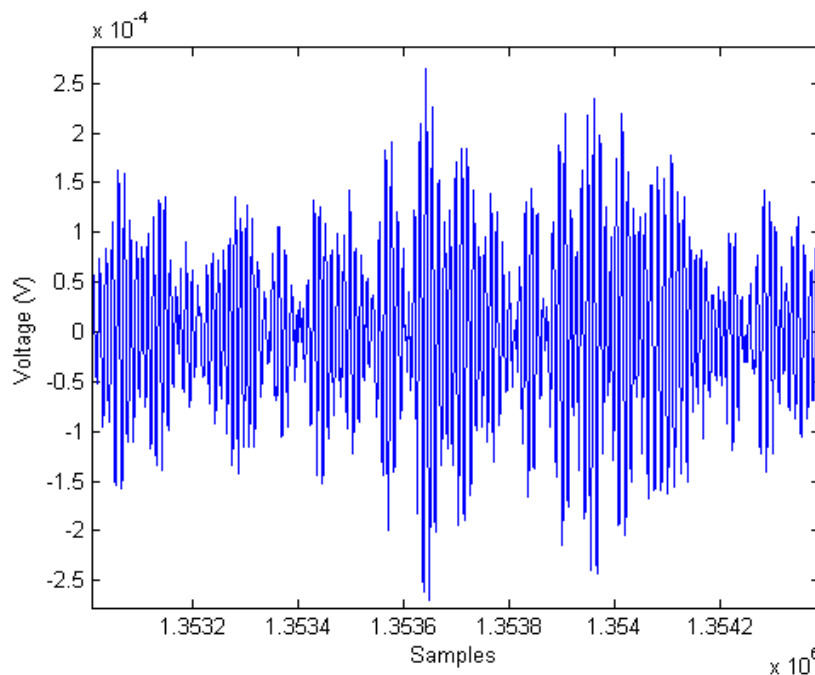


Figure 4.18 Disdrometer output for drops of size 0.3mm - 0.5mm along diameter

Unlike big drops (drop size $> 1\text{mm}$ along diameter), generating small drops is complex and requires a different setup. Also, generation of the small drops having fixed size requires a special facility lab. Therefore, the sizes of the drop are not fixed in the experiment but ranging from 0.3mm to 0.6mm along the diameter.

Furthermore, the momentum of these drops ranges from $24.4\mu\text{gm}\cdot\text{m/s}$ to $311\mu\text{gm}\cdot\text{m/s}$ (refer to Appendix C). For this range of momentum, the transfer function given in eq. 4.3 gives an expected output voltage ranging from $20.2\mu\text{V}$ to $258\mu\text{V}$. Figure 4.18 shows that the peaks of the signals range from $50\mu\text{V}$ to $260\mu\text{V}$.

Since, the size of the drops is not fixed in the experiment; it is difficult to infer if the small drops are following the same transfer function as the big drops. But the maximum peaks in the disdrometer's output are approximately equal to $260\mu\text{V}$. This value is very close to the calculated output voltage. This gives an indication that the small drops are following the same transfer function. But this does not provide enough evidence to make a firm conclusion and needs more research at special facilities where such small drops of fixed size can be generated individually.

Furthermore, the presented results suggest that drops of 0.3mm in diameter cannot be measured with the given transducer.

.

Chapter 5 Contributions and Recommendations

The current chapter discusses the original contributions of this work and makes a few recommendations for future work. Section 5.1 gives an overview of the contributions made. Subsequently, recommendations for future work are provided in Section 5.2.

5.1 Original Contributions

The presented work focused on characterizing the newly developed DWM disdrometer and designing a readout circuit for it. The original contribution made in the work are:

1. Earlier, the electrical characteristics of the DWM disdrometer were not well understood. To understand these properties and phenomenon, an equivalent electric model of the DWM disdrometer was developed and analyzed. The results shown in Section 3.2 confirm that this is an accurate equivalent electric model of the DWM disdrometer.
2. Previous to the presented work, the criteria for selecting the Piezoelectric Diaphragm (PED) for the DWM disdrometer was based on the desired catchment area. In Section 3.1.2 a PED selection criteria has been derived based on the PED's specifications like resonance frequency, thickness and catchment area.
3. In our experiments, it was observed that water gets accumulated on the top of the DWM disdrometer even after having conical shape hat. To solve the problem, a new hat with rounded edges has been proposed.
4. The DWM disdrometer suffers from the edge effect. It is a phenomenon where a raindrop impinges on the edge of the sensor surface and gives only a partial output. This results in an underestimation of the raindrop size. An elaborative analysis of this phenomenon has been done in Section 3.5. Based on this analysis, an innovative technique has been proposed and verified to remove the edge effect. The technique uses the envelope of the transducer's output to distinguish between drops that fall near the center of the disdrometer from drops that fall on the edge of the disdrometer.
5. A low-power (17.8mA@5V), low-noise (7.8 μ Vrms) readout circuit has been designed for the DWM disdrometer. This readout circuit was able to measure the drops of size as low as 0.4mm along the diameter. In the previous work [2], the minimum size of the drop measured has been reported to be 0.9mm along the diameter.
6. Table 5-1 gives a comparison of the designed DWM disdrometer with the commercially available disdrometer:

Table 5-1 Comparison with the commercially available disdrometer

Parameters	JWD	LPM	VR	DWM (this work)
Principle	Displacement	Optical	Acoustic	Acoustic
Range (raindrop size along diameter)	0.3 mm to 5 mm	0.16 mm to 8mm	1 mm to 5 mm	0.4 mm to 6 mm
Sampling Area	50 cm ²	46 cm ²	60 cm ²	10cm ²
Approx. Cost	\$ 12,000	US \$4,500	US \$2,500	US \$50 (Material cost)
Weight	5.1Kg	4.8 Kg	0.65 Kg	57gm
Dimensions	10 x 10 x 17 cm ³ (Sensor Unit) 12 x 26 x 27 cm ³ (Processing Unit)	27 x 17 x 54 cm ³	N.A	3.5 x 3.5 x7.5 cm ³
Power	115/230 Volts AC, 5.5 VA, (9 to 18 Volts DC; 3.3 Watts, also possible)	24 V AC /750 mA	3mA @ 12VDC (Stand by) Active – N.A.	17.8mA@5V (active) 1.3mA@5V (Stand by)

5.2 Future Recommendations

The following topics deserve to be subject of further study:

1. Currently, the proposed solution of the edge effect problem discards drops that hit on the edges of the sensor. This reduces the effective catchment area of the DWM disdrometer. It would be interesting to investigate if there is a relationship between the point of impact and the waveform pattern. This may enable us to use the edge drops instead of discarding them.
2. Currently, the transducer of the DWM disdrometer is a commercially available PED. This restricts the achievable performance from the disdrometer. Now, with the given understanding of the DWM disdrometer, a customized PED specifically for disdrometer can be developed.
3. The existing DWM disdrometer uses a PVC material for its casing. The properties of the PVC change with time and temperature. This directly affects the durability of the disdrometer. Therefore, it is worthwhile to study the effect of PVC material properties on the DWM disdrometer.
4. The sensitivity of the sensor needs to be investigated under different weather conditions.

Appendix A: Edge Detection Algorithm

The edge effect associated with the DWM disdrometer is discussed in the Section 3.5. Based upon the observation of the disdrometer output, a solution for the edge effect has been proposed in the Section 3.5.1. This appendix discusses the implementation details of the solution.

Figure A.1 shows an output of the disdrometer for a drop ('good drop') that hits near to the center of the sensor. The output is a damped sine wave having an exponentially decreasing envelope. Figure a.2 shows an output of the disdrometer for a drop ('edge drop') that hits on the edge of the sensor. As can be seen in the figure, the envelope of the signal generated by an edge drop cannot be defined. This property of the output signal has been used to distinguish a good drop from the edge drop.

For a "good drop", the difference between the upper envelope, $up(x)$ and the lower envelope, $down(x)$ should theoretically be a monotonically decreasing function.

$$\text{i.e., } f(x) = up(x) - down(x)$$

Where, $f(x)$ is a monotonically decreasing function as shown in Figure A.1. This property is used as the basis for implementation of the algorithm. The details are provided further.

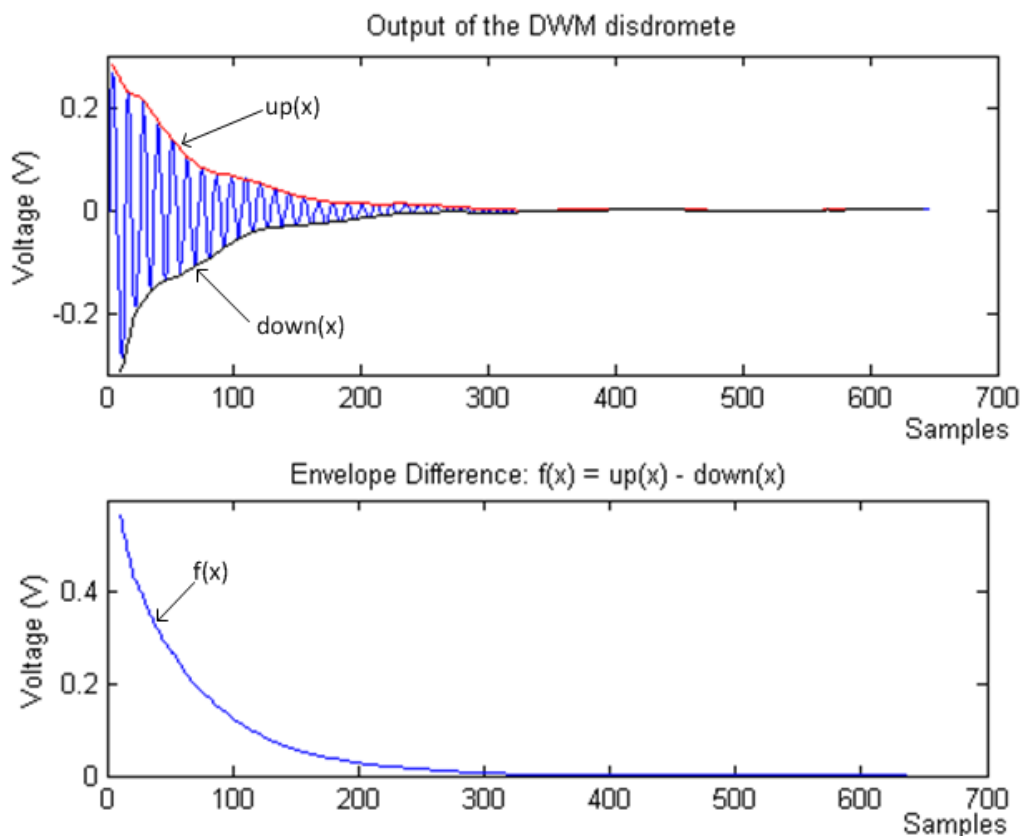


Figure A.1 Output of the DWM disdrometer for a drop hitting near the center of the sensor

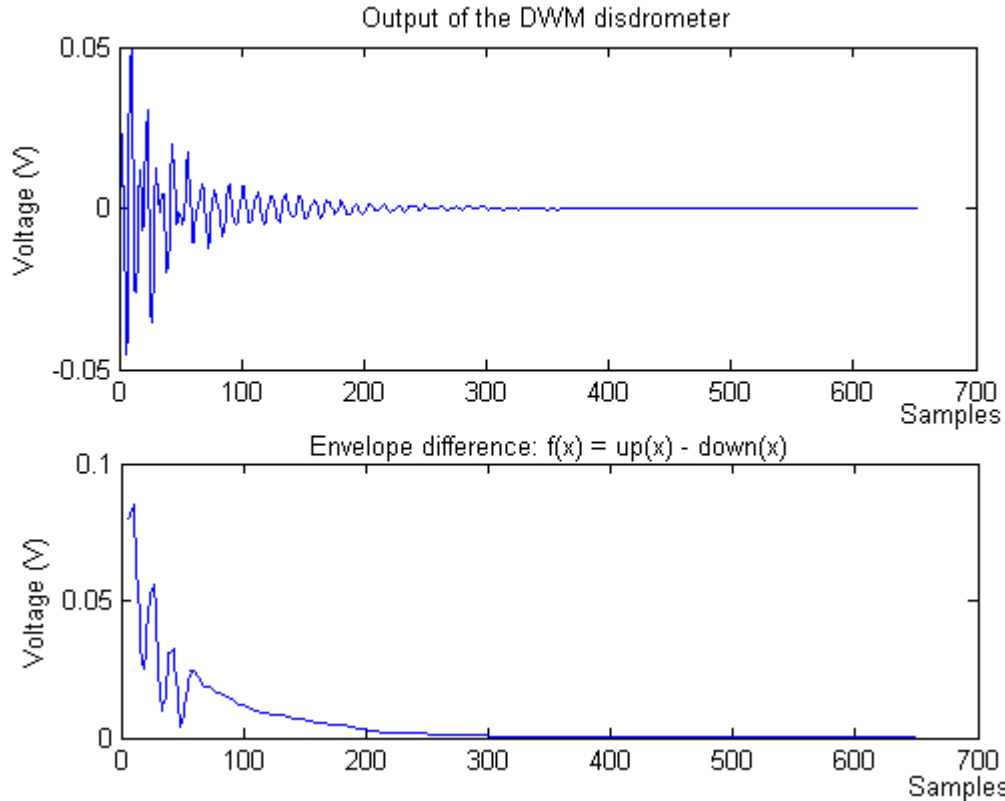


Figure A.2 Output of the DWM disdrometer for a drop hitting at the edges of the sensor

Even for good drops, experiments show that the function $f(x)$ sometimes demonstrates discontinuities. This effect is due to PED, packaging, mounting and glue. Therefore, the algorithm must have an error-tolerant design. The following are the possible discontinuities which may be present in the output signal for a good drop:

1. Ideally, for a good drop, $f(x+1)$ should always be less than $f(x)$. But, if the decay ratio is very high i.e. if,

$$\text{DecayRatio} = f(x+1)/f(x) < 0.6$$

It should be counted as an error.

2. At times $f(x+1)$ can be more than $f(x)$. But, if the difference is very small, for example if,

$$\text{HikeRatio} = f(x+1)/f(x) < 1.1,$$

The observed discontinuity should be ignored else it should be counted as an error.

3. For some really big drops, the HikeRatio can be as high as 1000 for the first 2-3 points. Figure A.3 shows this phenomenon. Therefore this should not be counted as an error.

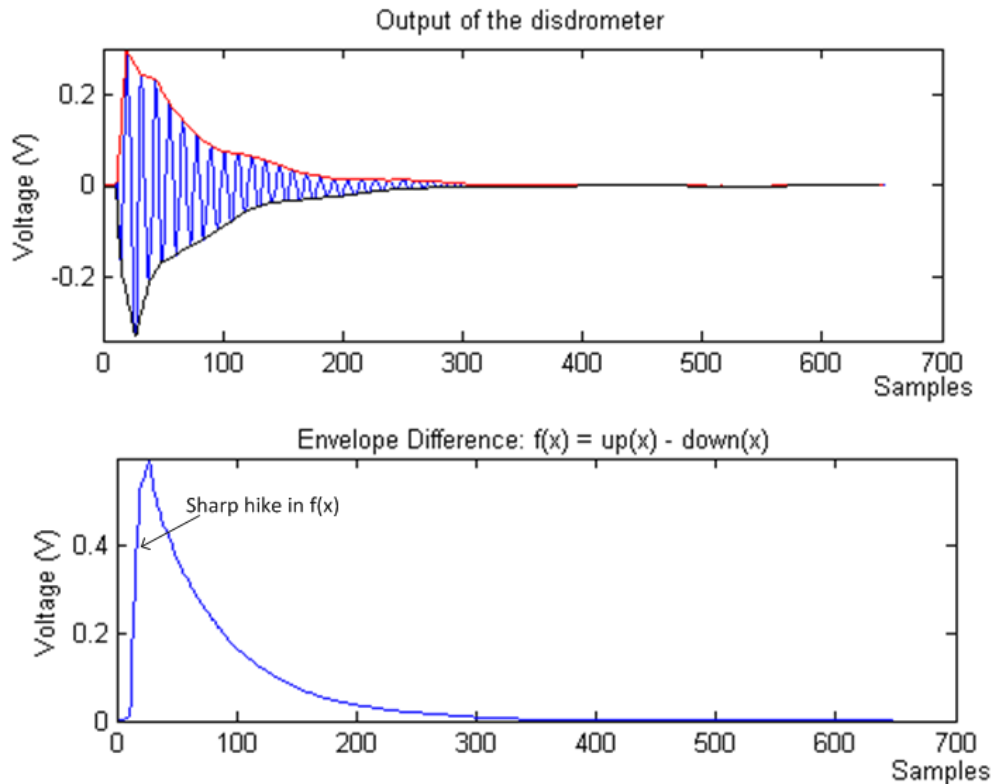


Figure A.3 Output of the DWM disdrometer for a good drop demonstrating the sharp hike in the function $f(x)$

Pseudo code of the algorithm:

Based on the above observations, the pseudo code of the proposed algorithm is as follow:

1. Extract the upper envelope 'up(x)' and down envelope 'down(x)' from the signal.
2. Calculate the function $f(x) = up(x) - down(x)$;
3. Check for small hikes:
 - if $f(x+1) > HikeRatio * f(x)$
 - $HikeFlag = HikeFlag + 1$;
4. Check for Sharpe hike at the initial of the signal:
 - if $f(x+1) > SharpHikeRatio * f(x)$ AND $x < 3$
 - $HikeFlag = 0$;
- 5 Check for the decay ratio:
 - if $f(x+1) < DecayRatio * f(x)$
 - $DipFlag = DipFlag + 1$;
6. To Tolerate few number of discontinuities
 - if $DipFlag > 2$ OR $HikeFlag > 0$
 - Edge drop;
 - else
 - Good drop;

Appendix B: Dynamic Range of the System

The Dynamic range (DR) of the readout circuit for the DWM disdrometer depends on the range of the raindrop's size. It is mentioned in Section 4.1.1 that the current work aims at measuring the raindrops with diameter ranging from 0.3mm to 6mm. Therefore, the needed DR of the readout circuit is defined as:

$$DR = 20 * \log \left(\frac{\text{output voltage for 6mm raindrop}}{\text{output voltage for 0.3mm raindrop}} \right)$$

The output voltage ' $V_0(D)$ ' of the DWM disdrometer for a raindrop of size 'D' along the diameter can be calculated using eq. 3.14. Repeating here for the reference:

$$V_0(D) = 0.82 * M_0(D)$$

where, $M_0(D)$ is the momentum of the raindrop of size 'D' along the diameter.

The momentum, $M_0(D)$, of the raindrop is given by eq. (2.4), Repeating here for the reference:

$$M_0(D) = m_0 v_0 = \frac{\rho \pi D^3}{6} \alpha D^\beta = \frac{\alpha \rho \pi D^{3+\beta}}{6}$$

where, $\rho = 1 \text{ gm/mm}^3$ is the density of a raindrop and 'D' is the diameter of the raindrop, $\beta = 0.67$ and $\alpha = 3.778 \text{ ms}^{-1} \text{ mm}^{-\beta}$ are empirically derived constants by [2].

Therefore the expected output voltage of the DWM disdrometer for raindrops of sizes 0.3mm and 6mm can be computed as:

$$V_0(0.3\text{mm}) = 19.4 \mu\text{V},$$

$$V_0(6\text{mm}) = 1.16\text{V}$$

So, the readout circuit needs to have a dynamic range of:

$$DR = 20 * \log \left(\frac{1.16}{19.4 * 10^{-6}} \right) = 98\text{dB}$$

Appendix C: Analysis of Available Power Budget

The assumptions used in the analysis are as follows:

1. Average duration of daylight per day: 8hr/day [45]
2. Blackout duration i.e. consecutive number of day without sunlight: 5days
3. On a rainy day, average number of hours of rainfall : 8hr/day
4. The backup battery for the blackout duration has efficiency equal to: 75%.
5. In the active mode, the DWM disdrometer consumes 40% power of the weather station.
6. A standard solar panel of 5W is being used for the weather station.
7. During the dry season, i.e. when it's not raining, the DWM disdrometer is in sleep mode and consumes negligible power.
8. In active mode, the DWM disdrometer has a power consumption of 'x' watt.
9. The remaining weather station has a power consumption of 'y' watt.

Thus,

$$y = \frac{(1-0.4)}{0.4} x = 1.5x$$

So, the power consumption of the weather station:

$$\begin{aligned} \text{During the rain event} &= x+y = x + 1.5x = 2.5x \\ \text{During the dry time} &= y = 1.5x \end{aligned}$$

Now, the energy generated by 5W solar panel is given by:

$$\text{Energy} = 5W * 8\text{hr/day} = 40\text{Whr/day}$$

During the blackout duration, the backup battery has to supply the power to the weather station. Therefore, if we use a battery of capacity 40Whr, the maximum available energy is given by:

$$\text{Available energy from the battery} = 40\text{Whr} * 0.75 = 30\text{Whr}$$

Furthermore, the average energy available per day during the blackout time can be computed as:

$$\text{Average energy per day during blackout} = 30\text{Whr}/5 = 6\text{Whr}$$

Now, it is assumed that the average number of hours of rainfall during the rainy season is 8hr/day. Thus, the DWM disdrometer is active for 8hr. For the remaining 16hr it is in sleep mode and consumes negligible power.

Therefore,

$$\begin{aligned} 8*(x+y) + 16*y &= 44x = 6W \\ &=> x = 136\text{mw} \end{aligned}$$

Thus, under the mentioned assumptions, the power consumption of the DWM disdrometer in the active mode should be less than 136mW. Therefore, 20mA@5V has been decided as the power specification for the readout circuit in our work.

Appendix D: Noise Analysis of the System

A complete analysis of the system noise is required in order to make an efficient readout circuit. The current appendix discusses the noise budget analysis of the readout circuit for the DWM disdrometer.

The analysis is based on the following considerations:

1. The readout circuit is powered by 2.5V ($=V_{cc}$)
2. The biasing voltage of opamp is 1.25 V
3. ADC has a resolution of 24bits
4. Bandwidth of the system is 10 kHz ($=BW$)
5. Depending on the transducer used, the output voltage of the DWM disdrometer can be as large as 1.2 V. Therefore, the gain of the amplifier is assumed to be 1 ($=Gain$) in order to do the noise analysis for the worst case scenario
6. The current noise of the amplifier is very low and has been ignored in the analysis

There are four sources of noise in the DWM disdrometer system, namely:

1. Piezoelectric diaphragm
2. Amplifier
3. Feedback resistors
4. Analog-to-Digital Converter

Figure D.1 shows the noise model of the circuit:

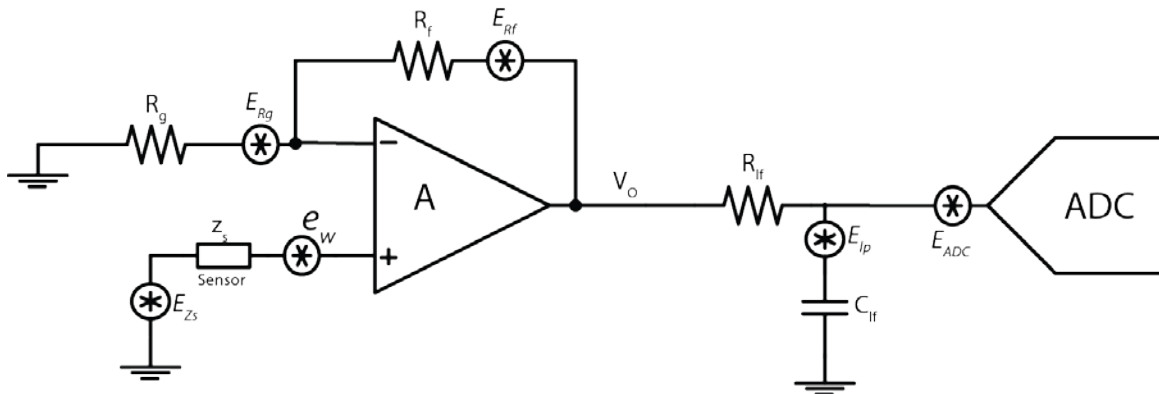


Figure D.1 Noise Equivalent circuit of the proposed design

In the analysis:

1. NBW represents the noise bandwidth of the system which is equal to $1.57 \cdot BW$.
2. NG represents the noise gain which is equal to the 'Gain' of the amplifier

3. The gain of the system is given by $\text{Gain} = (1 + \frac{R_f}{R_g})$

Therefore, for the given circuit:

Output referred noises of the resistors are given by:

$$\text{Noise of } R_g = E_g^2 = 4kTR_g(NBW)(\frac{R_f}{R_g})^2$$

$$\text{Noise of } R_f = E_{R_f}^2 = 4kTR_f(NBW)$$

Output referred Noise of the given sensor:

$$\text{Noise of } Z_s = E_{Z_s}^2 = 4kTZ_s(NBW)(1 + \frac{R_f}{R_g})^2$$

The total output referred noise of resistors and sensor is given by:

$$E_{out,rms} = \sqrt{E_{R_f}^2 + E_{R_g}^2 + E_{Z_s}^2}$$

Therefore, the input referred noise because of the resistors and the sensor is given by

$$E_{R,rms} = \frac{E_{out,rms}}{NG}$$

$$E_{R,rms} = \sqrt{4k_B T(NBW) \left[\frac{R_f R_g}{R_g + R_f} \right] + R_s}$$

where, k_B is the bolt Boltzmann constant

T is the Temperature

Noise due to Op-Amp:

Assuming, the power spectral density of the Op-amp is given by e_w

The noise at the input of the amplifier is given by:

$$E_{op,rms} = \sqrt{e_w^2 \left(f_{nc} * \ln \left(\frac{f_H}{f_L} \right) + NBW \right)}$$

where, f_H = High cutoff frequency

f_L = Low cutoff frequency

f_{nc} = Knee frequency

Noise due to Low pass filter:

The input referred noise of the low-pass filter between the amplifier and the ADC is given by:

$$E_{lp,rms} = \sqrt{\frac{k_B T}{C_{lp}}} / NG$$

Noise due to ADC:

An ADC has two types of noise: Quantization noise and Thermal noise.

The quantization noise of an ADC is given by: $E_{quant}^2 = \frac{q^2}{12}$, where, q is the LSB.

Since, $E_{th,adc}$ represents the thermal noise floor of the ADC, the input referred noise due to the ADC is given by

$$E_{ADC,rms} = \frac{\sqrt{(E_{quant}^2 + E_{th,adc}^2) * NBW}}{NG}$$

Total input referred noise of the system:

Therefore, the total input referred noise of the system is given by:

$$E_{rms} = \sqrt{(E_{R,rms}^2 + E_{op,rms}^2 + E_{lp,rms}^2 + E_{ADC,rms}^2)}$$

For the worst case, i.e. Gain = 1:

1. $NG = 1$
2. $R_f = 0$ and $R_g = \infty$

Also, given is:

1. $NGB = 1.57 * BW = 1.57 * 10kHz = 15.7kHz$
2. $Z_s = 10\Omega$

Assuming:

1. $C_{lp} = 0.1\mu F$
2. $e_w = 15nV/\sqrt{Hz}$, $f_{nc} = 1kHz$
3. $E_{th,adc} = 30nV/\sqrt{Hz}$

With these given values, the input referred noise of the complete system is computed to be:

$$V_n = 6.9\mu V_{rms}$$

The calculated input referred noise matches with the specification of $7\mu V_{rms}$ for the noise mentioned in Section 4.1.3.

Noise calculation of the implemented system:

The resonance frequency of the DWM disdrometer, which has been used during the presented work, is at 5.8 kHz and does not requires a bandwidth of 10kHz. Therefore, a bandpass filter has been used to filter the out of band noise. It has a low frequency cutoff at 2kHz and the upper cutoff frequency at 8.5kHz. Therefore, for the given system:

1. V_{ref} of the ADC is 2.5V
2. Gain = 1
3. BW = 6.5kHz
4. $C_{lp} = 0.1\mu F$
5. $e_w = 11 \text{ nV}/\sqrt{\text{Hz}}$, $f_{nc} = 1\text{kHz}$, $f_L = 2 \text{ kHz}$, $f_H = 8.5\text{kHz}$
6. $E_{th,adc} = 30\text{nV}/\sqrt{\text{Hz}}$

For the given values, the input referred noise of the system should be:

$$V_n = 5.67\mu V_{rms}$$

Bibliography

- [1] Project Website: <http://www.tahmo.org>, Last login: 16:25hr, Feb 2, 2012.
- [2] Jong, S. de, 2010. "Low cost disdrometer: Improved design and testing in an urban environment.", Master Thesis, Delft University of Technology.
- [3] Jayawardena, A.W., Rezaur, R.B., 2000. "Drop size distribution and kinetic energy load of rainstorms in Hong Kong.", *Hydrological Processes*. 14, 1069–1082.
- [4] Pearson, J. E., Martin, G. E., 1957. "An Evaluation of Raindrop Sizing and Counting Techniques.", Illinois State Water Survey and University of Illinois, Scientific Report No. 1.
- [5] Distromet Ltd., <http://www.distromet.com>, Last login: 13:38hr, Feb 2, 2012.
- [6] Distromet Ltd., "Disdrometer RD-80", Instruction Manual, June 20, 2002
- [7] Distromet Ltd., <http://www.distromet.com/64/Support.html>, Last login: 13:42hr, Feb 2, 2012.
- [8] Lavergnat, J., Golé, P. 1998. "A Stochastic Raindrop Time Distribution Model." *Journal of Applied Meteorology* 37, 805-818.
- [9] Thies CLIMA, <http://www.thiesclima.com/disdrometer.html>, Last login 13:47hr, Feb 2, 2012.
- [10] Salmi, A., Elomaa, A., Kopsala, P., Laukkanen, E., "Piezoelectric Vaisala raincap sensor applied to Drop Size Distribution monitoring".
- [11] http://www.geneq.com/catalog/en/wt_wxt520.html, Last Login: 14:05, Feb 2, 2012.
- [12] Vaisala, "WXT520 Vaisala Weather Trasmmitter", Doc M210906EN-B .
- [13] Degen, C., Hut, R., Giesen, N. van de, 2009., "Disdrometers Article", Delft University of Technology.
- [14] Montero-Martínez G, Kostinski AB, Shaw RA, García-García F., 2009. "Do all raindrops fall at terminal speed?" *Geophys. Res. Lett.*, 38, L11818, doi:10.1029/2008GL037111
- [15] Beard, K. V., Chuang, C., 1987. "A New Model for the Equilibrium Shape of Raindrops." *Journal of the Atmospheric Sciences* 44, 1509-1524.
- [16] [http://en.wikipedia.org/wiki/Drop_\(liquid\)](http://en.wikipedia.org/wiki/Drop_(liquid)), Last login: 13:58hr, Feb 2, 2012
- [17] Beard, K. V., 1976. "Terminal Velocity and Shape of Cloud and Precipitation Drops Aloft." *Journal of the Atmospheric Sciences* 33, 851 - 864.

- [18] Laws, J. H., 1941. "Measurement of the Fall-Velocity of Water Drops and Rain Drops.", Trans. of the American Geophysical Union, 22, 709 – 721.
- [19] Gunn, R., Kinzer, G. D. 1949. "The Terminal Velocity of Fall for Water Droplets in Stagnant Air." Journal of Meteorology 6, 243 - 248.
- [20] Beard, K. V., Pruppacher, H. R., 1969. "A determination of the terminal velocity and drag of small water drops by means of a wind tunnel." Journal of Atmospheric Sciences 26, 1066–1072.
- [21] Uijlenhoet, R., Stricker, N. M., 1999. "A Consistent Rainfall Parameterization based on the Exponential Raindrop Size Distribution." Journal of Hydrology 218, 101 - 127.
- [22] Winder, P. N., 2010., "An Acoustic Water Tank Disdrometer", PhD dissertation, The University of Hull
- [23] Aurelien, "The Piezoelectric Effect", PZT Application Manual
- [24] Jordan, T. L., Ounaies, Z., 2001. "Piezoelectric Ceramics Characterization, National Aeronautics and Space Administration (NASA).", ICASE Report No. 2001-28.
- [25] Physik Instrumente, "Fundamentals of Piezoelectricity", Piezo Actuator Tutorial, Last login: 10:23hr, Jan 23, 2012.
- [26] Degen, C., 2009. "Development of a Low-cost Acoustic Rain Gauge.", Internship report, Delft University of Technology.
- [27] Physik Instrumente, "Dynamic Forces", Piezo Actuator Tutorial, Last login: 10:52hr, Jan 23, 2012.
- [28] IEEE Standard on Piezoelectricity, 176-1987, The Institute of Electrical and Electronic Engineers.
- [29] Goldfarb, M., Celanovic, N., 1997. "A Lumped Parameter Electromechanical Model for Describing the Nonlinear Behavior of Piezoelectric Actuators", ASME Journal of Dynamic Systems, Measurement, and Control 119, 478-485.
- [30] Goldfarb, M., Jones, L. D., 1999. "On the efficiency of electric power generation with piezoelectric ceramic", ASME Journal of Dynamic Systems, Measurement, and Control 121, 566-571.
- [31] Sherrit S., Wiederick H.D., Mukherjee B.K., Sayer M. 1997. An Accurate Equivalent Circuit for the Unloaded Piezoelectric Vibrator in the Thickness Mode, Journal of Physics D: Applied Physics 30, 2354-2363.

- [32] C. H. Park, 2001. "On the circuit model of piezoceramics", *Journal of Intelligent Material Systems and Structures* 12, 515-522.
- [33] Guan, M., Liao, W. H., 2004, "Studies on the circuit models of piezoelectric ceramics.", *Proceedings International Conference on Information Acquisition*, 26- 31.
- [34] Förster, J., Gust, G., Stolte, S., 2004. "A Piezoelectrical Rain Gauge for Application on Buoys." *Journal of Atmospheric and Oceanic Technology* 21, 179–193.
- [35] Nearing, M. A., Bradford, J. M., Holtz, R. D., 1986. "Measurement of Force vs. Time Relations for Waterdrop Impact." *Soil Science Society American Journal* 50, 1532–1536.
- [36] Umeda, M., Nakamura, K., Ueha, S., 1996. "Analysis of the transformation of mechanical impact energy to electric energy using piezoelectric vibrator", *Japan. Journal of Applied Physics* 35, 3267-73.
- [37] Licznar, P., Lomotowski, J., Blonski, S., Ciach, G.J., 2008. "Microprocessor field impactometer calibration: do we measure drops' momentum or their kinetic energy?" *Journal of Atmospheric and Oceanic Technology* 25, 742–753.
- [38] Jayawardena, A. W., Rezaur, R. B., 2000. "Measuring drop size distribution and kinetic energy of rainfall using a force transducer" *Hydrological Processes* 14, 37-49.
- [39] Texas Instruments, "Signal Conditioning Piezoelectric Sensors", Application Report SLOA033A
- [40] Turo A., Salazar, J., Chavez, J. A., Kichou, H. B., Gomez, T. E., Montero de Espinosa, F., Garcia-Hernandez, M. J., 2003. "Ultra-low noise front-end electronics for air-coupled ultrasonic non-destructive evaluation.", *NDT and E International* 36, 93-100.
- [41] Yañez, Y., Garcia-Hernandez, M. J., Salazar, J., Turo, A., Chavez, J. A., 2005. "Designing amplifiers with very low output noise for high impedance piezoelectric transducers.", *NDT and E International* 38, 491-496.
- [42] Texas Instruments, LMV851 Low power CMOS Amplifier, Oct 2007.
- [43] Analog Devices, "AD7767 24-Bit, Oversampled SAR ADC, Rev C, May 2010.
- [44] Maxim, "Max6126 Ultra-High-Precision, Ultra-Low-Noise, Series Voltage Reference", Rev 5, Dec 2010.
- [45] <http://astro.unl.edu/classaction/animations/coordsmotion/daylighthouseexplorer.html>, Last login: 12:39hr, March 23, 2012.
- [46] Joss, J., Waldvogel A., 1977, "Comments on Some observations on the Joss-Waldvogel rainfall disdrometer". *Journal of Applied Meteorology*, 16, 112-113.

- [47] Salmi, A., Elomaa, L., 2007. "Measurements of the Terminal Velocity and Shape of Falling Raindrops at Vaisala Rain Laboratory", 8th European Conference on Application of Meteorology (ECAM), San Lorenzo de El Escorial, Spain.
- [48] Murata Manufacturing Company, Ltd, "Piezoelectric Sound Components" Application Manual, Doc P15E.pdf, 07.10.17.